PHOTOELECTRON SPECTROSCOPY OF CLUSTER ANIONS: ELECTRON INDUCED PROTON TRANSFER, SOLVATED MOLECULES, AND CO_2 ACTIVATION BY ANION CLUSTERS

by

Yi Wang

A dissertation submitted to The Johns Hopkins University in conformity with

the requirements for the degree of Doctor of Philosophy

Baltimore, Maryland

October, 2015

Abstract

My research of interests are focused on gas phase anion clusters. The experimental method utilized in this dissertation is negative anion photoelectron spectroscopy (PES). Anion photoelectron spectroscopy is conducted by crossing a mass-selected beam of negative ions with a fixed-frequency photon beam and energy-analyzing the resultant photodetached electrons. It is especially useful to study interactions between molecules. In this dissertation, several interesting interaction between molecules are investigated. The photoelectron spectroscopic study of Quinoline$^-$ shows that it displays a greater electrophilicity than its analog, naphthalene. The substituted nitrogen on its ring provides quinoline the ability to support a valence bound anion. The interaction between quinoline- and CO_2 was further investigated. Because of the lone electron pair on the nitrogen, the stable CO_2 linear structure can be bent and stabilized by the conjugated ring. In the hydrated N-heterocylic system, five molecule were examined ranging from one nitrogen substituted to three nitrogen substituted rings, including pyridine, pyrimidine, pyridazine, pyrazine, and s-triazine. Heterocyclic rings with only 1 or 2 nitrogen atoms have negative electron affinities, but the addition of solvating water molecules can yield stable

negative ions. A very important electron induced proton transfer process from water to pyridine was observed for the first time, despite the fact that water can be considered as a weak acid and not willing to give up a proton. Electron-induced proton transfer occurs in many biology related reactions. The 2-hydroxypyridine dimer had been studied both experimentally and theoretically. Experimental and theoretical findings confirm that the proposed intermolecular electron induced proton transfer process occurs in the dimer anion.

Readers:

Dr. Kit H. Bowen

Dr. Harris Silverstone

Dr. Arthur Bragg

Acknowledgement

First of all, I would like to thank my academic adviser, Dr. Kit Bowen. In the summer 2009, when I was first introduced in his lab, I was fascinated by the amazing scientific equipments. I had a wonderful and fulfilling time, which led me to continue my research career as a PhD student in Dr. Bowen's group the year after. Through all the years under working in his research group, he impressed me with his breadth of chemistry knowledge. More importantly, his passion in science deeply influenced everyone in the lab.

Soren Eustis and Andrej Grubisic were the most senior group member when I entered the group. They had been great role models as mature young scientists. Xiang Li was another senior group member in my early years. His optimistic personally and sense of humor made my time working under his supervision very enjoyable. Di Wang is a great friend to talk to and she is very outgoing. I have never worked with Jae Ko, but he gave me useful fashion advises. Haopeng Wang is a very hardworking and serious scientist. He is a quiet guy but whenever he speaks, his word is always precise and valuable. Jing Chen is a great friend and in the same time, she is my mentor on the SNIPES machine. Besides science, we shared a lot about life too. Me and Angela had been worked together for two years. I learnt a lot from her not only the SNIPES secrets, but also baseball and movies. Allyson and Jacob are the "working horses" on PSA. I was deeply impressed by their work on their machine. Xinxing Zhang is a great prosperous young scientist. He is a great friend too. I will miss the time we spent together these years. Xin Tang is a very smart and hardworking guy. He spends so much time in the lab so that someone would think "does he live in the lab?" Evan Collins is a very energetic and easy going guy. I hope the ESI

apparatus he has been building these years will have great outcomes. Zachary, Sandy, Nic and Gaoxiang are the youngest generation of our lab. They turned learning mode to research mode rapidly. I wish my best to their future.

I want to thank my thesis committee members, Dr. Harris Silverstone, and Dr. John Toscano. Thank you for giving me great advises in my department oral and GBO.

Finally I want to thank my family. My parents have been always supporting me. Especially my mother, who passed away several months ago. How I wish she be with me when I finally become a PhD. I truly miss you and you are always be in my heart.

Table of Contents

List of Figures

List of Tables

Chapter 1. Introduction

1.1 Overview

The physical and chemical properties of individual atoms and molecules are often very different from the bulk material. Clusters, by definition, are the aggregates of atoms and molecules formed by interaction. The size of the clusters can range from single to hundreds. The investigation of the clusters provides the opportunity to unravel the evolution of the properties and behaviors from microscopic to macroscopic world. In addition, the characteristics of clusters their selves are unique and can change dramatically even with small incremental change in size.

In exploring the unique properties of cluster ions, mass spectrometry is a useful analytical technique to investigate the composition and structural information of the cluster ions. For example, in comparing the effectiveness of different 5-substituted uracils, theoretical calculations predicted that 5-thiocyanouracil would undergo dissociative electron attachment. It could be employed in human cancer radiotherapy if they could be sensitized to dissociate upon reaction with hydrated electrons. Mass spectroscopic study shows that the parent anion is not observed on the spectrum, while the fragment, SCN^- had a strong signal intensity. Therefore 5-thiocyanouracil is a good candidate as a radiosensitizer for cancer treatment.

Although mass spectrometry can provide the structural information of the clusters, it is not sufficient to give the information of electronic structure of the cluster. The primary tool used in the this dissertation to investigate the electronic structures of the clusters is anion photoelectron spectroscopy (PES). Negative ion photoelectron spectroscopy is conducted by crossing a mass-selected beam of anions with a fixed-frequency photon beam and energy-analyzing the resultant photodetached electrons. In photoelectron spectroscopy experiments,

electron binding energy is measured, governed by the energy conservation relation: hυ=EKE+EBE, where hυ is the photon energy, EKE is the electron kinetic energy, EBE is the electron binding energy. Anion photoelectron spectrometry is especially good at study the interaction of electrons and neutral moieties, namely electron affinity. Electron affinity is an important property of atoms and molecules. The stability of anions are of great importance in many chemistry, biology, material science area, including biological pathways of electron transfer, low energy attachment induced DNA pair leakage, and semiconductor chemistry.

In figure.1 the energies associated with electron affinity (EA) are summarized and illustrated. The transition between neutral and anion vibrational ground states is often referred as the adiabatic electron affinity (AEA). However, due to the limitation of spectroscopy experiments, the (0,0) transition is not always observable. Thus the vertical detachment energy (VDE) is often measured, which is corresponding to the most intense Franck-Condon features of the detachment spectrum. Vertical attachement energy (VAE), on the other hand, is usually not experimentally determined but always calculated by theoretical methods. The physical interpretation of VAE is the energy of attaching an electron to the neutral with little geometry change to it. In theoretical calculations, all three energies can be calculated in terms of the geometry optimizations.

$$AEA = E_{Neutral}(\text{optimized geometry}) - \text{Energy}_{Anion}(\text{optimized geometry})$$

$$VDE = E_{Neutral}(\text{optimized geometry of anion}) - \text{Energy}_{Anion}(\text{optimized geometry})$$

$$VAE = E_{Neutral}(\text{optimized geometry}) - \text{Energy}_{Anion}(\text{optimized geometry at neutral})$$

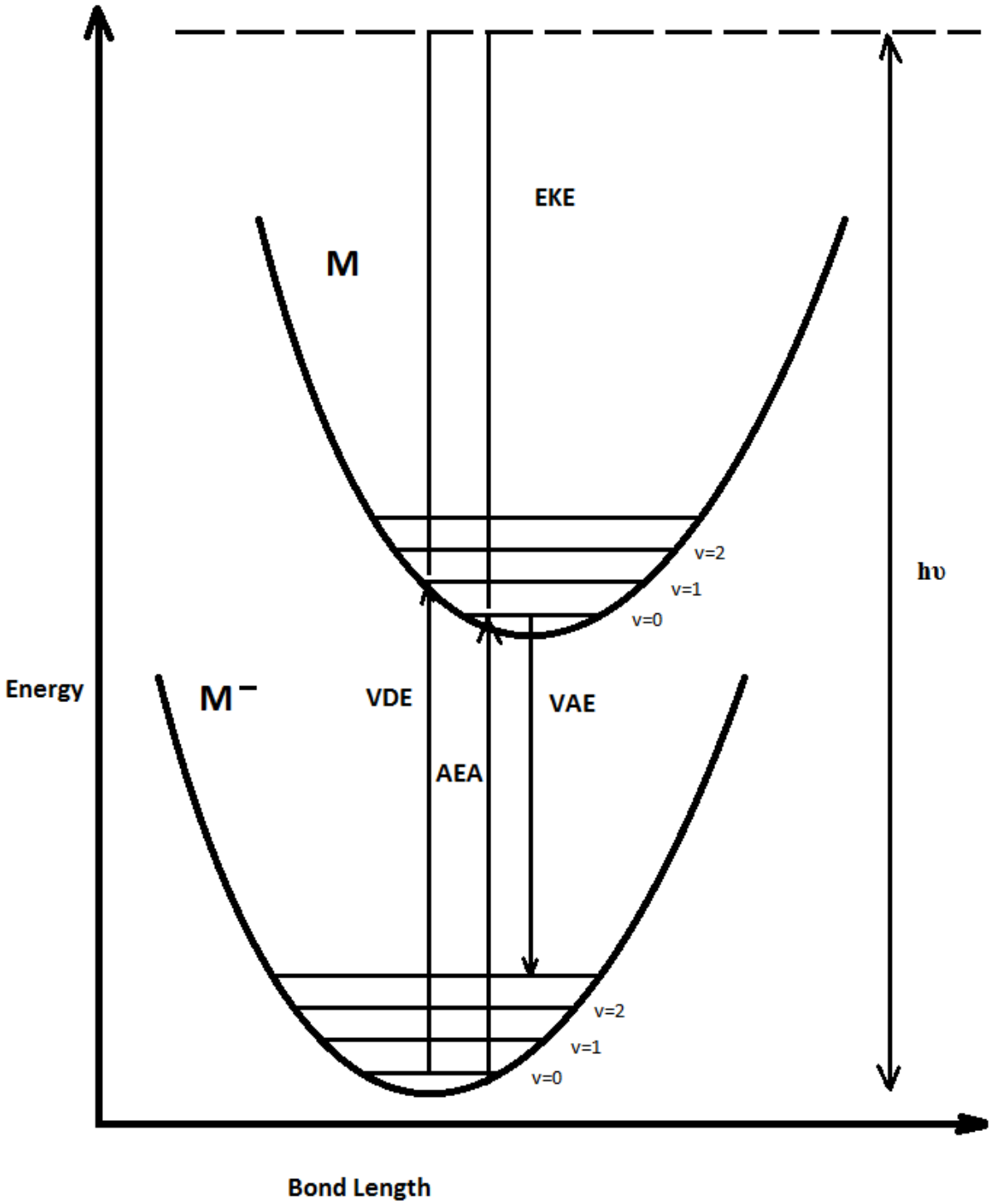
EKE
M
v=2
v=1
v=0
hυ
Energy
M⁻
VDE
VAE
AEA
v=2
v=1
v=0
Bond Length

Figure 1.1 Energy Diagram in Photoelectron Spectroscopy

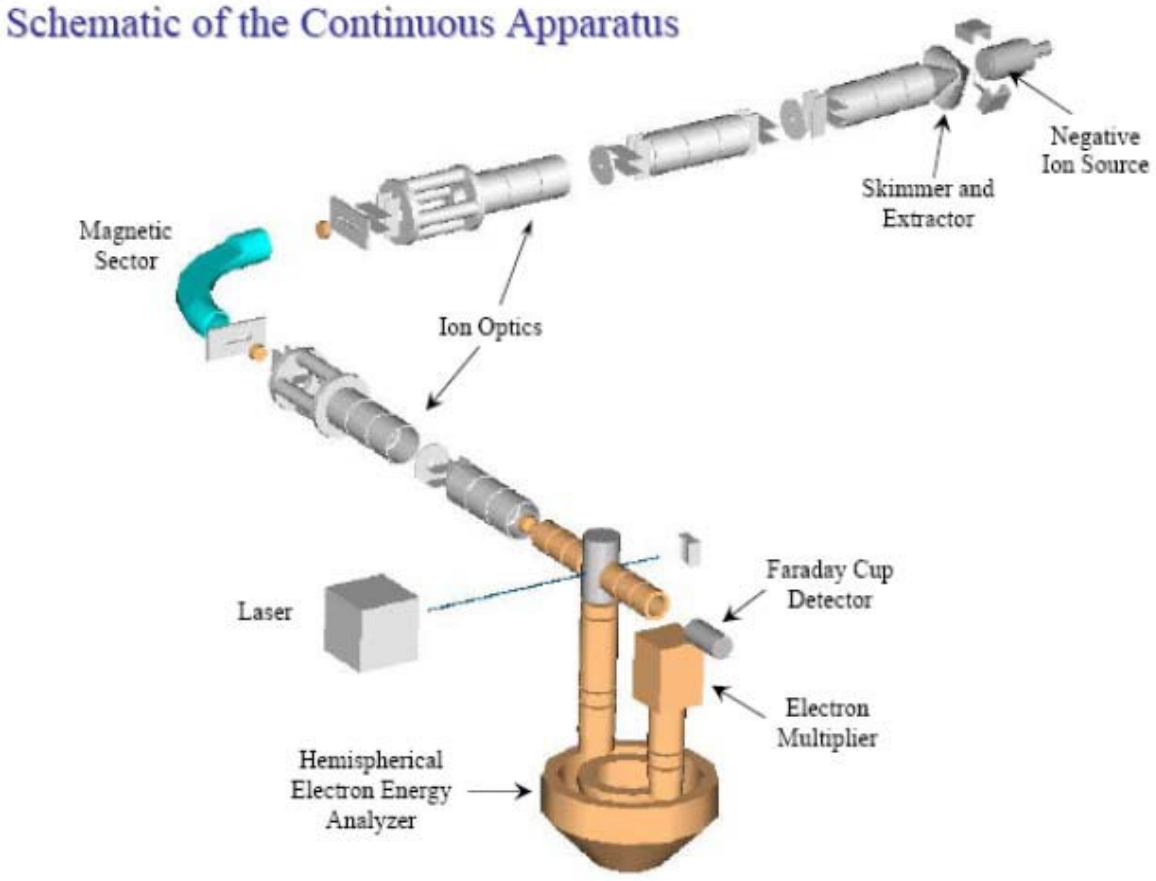

Figure 1.2 SNIPES Apparatus Scheme

1.2 SNIPES Apparatus

The Ion Source

There are many ion sources can be equipped in SNIPES. The most frequently used one is the supersonic expansion nozzle ion source. In this thesis, all the experiments were performed with this source. Negative ions are formed by expand a gas mixture at a pressure of one to four atmosphere through a small orifice, usually 10 to 50 micron diameter into a high vacuum chamber, usually 10^{-5} to 10^{-4} Torr. The stagnation chamber is equipped with temperature control cooling/heating jacket as well as a heating wire coil, such that the temperature can be varied from liquid nitrogen temperature (-197°C) to upper temperature limit of the o-ring seal (~200°C) . A hot negatively biased filament (Th/Ir for oxidizing gases and Th/W for reducing gases) is placed immediately next to the nozzle, emitting electrons to make anions, in the presence of an axial magnetic field (produced by three -200 G magnets). After anions are formed, they are confined and extracted by a skimmer, carried downstream.

Mass Spectrometry

Before photoelectron spectroscopic analysis, anions of interest should be carefully mass-selected. The mass spectrometer equipped on SNIPES is a magnetic sector, which uses an electromagnet to separate ions based on their deflection due to a homogeneous magnetic field.

Magnetic sector mass analyzers make use of the fact that a centripetal force on an ion in a homogenous magnetic field is of the form:

$$\mathrm{KE} = \frac{1}{2}mv^2 = qV. \qquad (1)$$

Where m is the mass of the cluster anion, v is the velocity, q is the charge (in our experiment, due to the low electron energy emitted, q is almost exclusively negative one), and V is the beam voltage, usually -500V. Thus, the kinetic energy of the incoming cluster anions is at 500eV despite the mass of the cluster anions.

When the cluster anions enter into the homogenous magnetic field, they feel a magnetic force perpendicular to the direction of the velocity of the cluster anions. The result is magnetic force balanced with the centrifugal force and therefore the motion is circular. The beauty of the magnetic field is it does no work on the anions, therefore the anions of interest can be selected according to their velocity. The equation describes the balance of magnetic field force and centrifugal force is shown as:

$$F_c = \frac{mv^2}{r} = F_B = Bvq \quad (2)$$

Where F_c is the centrifugal force, F_B is the magnetic force, and B is the magnetic field. Rearrange this equation, we obtain the mass-to-charge ratio:

$$\frac{m}{q} = \frac{Br}{v} \quad (3)$$

From the equation 1, we got $v = \sqrt{\frac{2Vq}{m}}$, substitute into equation (3) and rearrange, we got:

$$\frac{m}{q} = \frac{B^2 r^2}{2V} \quad (4)$$

Since the charge q, radius of the magnet r, and beam voltage V are known and constant in the experiment, the mass of the cluster anion m, is proportional to the magnetic field, B to the second order. The operation details can be found in the Appendix II.

1.3 System Explored

Water solvated N-heterocylic Cluster

In the hydrated N-heterocylic system, five molecules were examined ranging from one nitrogen substituted to three nitrogen substituted rings, including pyridine, pyrimidine, pyridazine, pyrazine, and s-triazine. Heterocyclic rings with only 1 or 2 nitrogen atoms have negative electron affinities, but the addition of solvating water molecules can yield stable negative ions. In the case of the diazines ($C_4H_4N_2$), pyrazine, pyrimidine, and pyridazine, the addition of one water molecule is enough to stabilize the negative ion, with the majority of the excess electron density in a π^* orbital of the heterocycle but not significantly extended over the hydrogen bonded water network. Pyridine (C_5H_5N), with the most negative electron affinity, requires three water molecules to stabilize its negative ion. Also, a very important electron induced proton transfer process from water to pyridine was discussed. Bowen group has been the leader of investigating electron-induced proton transfer. However, this is the first time we observed water as a proton donor, despite the fact that water can be considered as a weak acid and not willing to give up a proton.

Electron-Induced Proton Transfer in DNA like molecules.

Electron-induced proton transfer occurs in many biology related reactions. When low-energy electrons are produced by ionization as a result of high-energy radiation, the excess electron is likely to attach onto a DNA base pair leading to barrier-free proton transfer. Such a

process has been suggested as the key step in DNA tautomerization and considered to be the cause of damage to DNA molecules in cells. The 2-hydroxypyridine dimer had been studied both experimentally and theoretically, due to its structural similarity to DNA base pairs. Experimental and theoretical findings confirm that the proposed intermolecular electron induced proton transfer process occurs in the dimer anion.

CO2 Activation

Some years ago, Kim and coworkers found that bonding took place between the carbon atom in CO2 and a nitrogen atom in its heterocyclic molecular partner. From a Lewis acid-base perspective, the heterocycle's nitrogen atom, i.e., its lone electron pair, was the electron donor and CO2 was the electron acceptor, both well-known properties of these constituents. As neutral adducts some degree of binding would have been expected, but with the addition of excess electrons, robust binary anionic complexes. We examine the covalent bonding between a unique heterocyclic molecule, Quinoline, and CO2. In this work, the bonding energy of the (Quinoline-CO2)- were determined by utilizing mass spectrometry, photoelectron spectroscopy, and density functional calculations.

Quinoline Valence Anion

Aside from (Quinoline-CO2)- anion complex, quinoline itself forms stablize anion. Typically, cyclic aromatic hydrocarbons such as benzene and naphthalene as well as their heteroaromatic analog structures do not support a valence bound anion. Quinoline displays a

greater electrophilicty than its analog, naphthalene, due to the presence of substituted nitrogen. A small but positive electron affinity of 0.16 eV was experimentally measured, indicating that quinoline supports a valence bound anion. Also, vibrationally-resolved anion photoelectron spectrum of quinoline− anion is supported by our theoretical calculations and computationally simulated spectrum.

1.4 References

(1) Bacic, Z.; Miller, R. E. *J. Phys. Chem.* 1996,*100,*12945.

(2) Sugano, S.; Koizumi, H. *Microcluster Physics, Second Edition-,* Springer, 1998.

(3) Crawford, O. H.; Dalgarno, A. *Chem. Phys. Lett.* 1967,*1,* 23.

(4) Eustis, S. N.; Radisic, D.; Bowen, K. H.; Bachorz, R. A.; Haranczyk, M.; Schenter, G. K.; Gutowski, M. *Science (Washington, DC, U. S.)* 2008, *319,* 936.

(5) Eustis, S. N.; Whiteside, A.; Wang, D.; Gutowski, M.; Bowen, K. H. *J. Phys. Chem. A* 2010,*114,* 1357.

(6) Coe, J. V. *PhD. Dissertation* 1986.

(7) Snodgrass, J. T. *PhD. Dissertation* 1986.

(8) Freidhoff, C. B. *PhD. Dissertation* 1987.

(9) McHugh, K. M. *PhD. Dissertation* 1988.

(10) Lippa, T. P. *PhD. Dissertation* 1998.

Chapter 2. Photoelectron Spectrum of a Polycyclic Aromatic Nitrogen Heterocyclic Anion: Quinoline$^-$

A. M. Buytendyk, Y. Wang, J. D. Graham, A. K. Kandalam, B. Kiran and K. H. Bowen

We report a joint photoelectron spectroscopic and theoretical study on the molecular anion, quinoline$^-$. Analysis of the vibrationally resolved photoelectron spectrum found the adiabatic electron affinity, $EA_a(C_9H_7N)$, to be 0.16 ± 0.05 eV. These findings were supported by density functional theory calculations. Our experimental and computational results demonstrate the unusual electrophilicity for a polycyclic aromatic heterocycle.

Keywords: Molecular anion; Electron affinity; Photoelectron spectroscopy; Gas phase; Density functional theory

2.1 Introduction

Typically, cyclic aromatic hydrocarbons such as benzene and naphthalene as well as their heteroaromatic analog structures do not support a valence bound anion. Quinoline is a polycyclic aromatic nitrogen heterocycle that is structurally equivalent and π-isoelectronic to naphthalene, where a nitrogen atom replaces the position 1 CH group on the hydrocarbon. Semi-empirical calculations predicted a small *positive* electron affinity for quinoline almost fifty years ago[1]. The neutral quinoline molecule has been extensively studied computationally[2-9] and experimentally in the gas phase by measuring the dielectric constant to determine the dipole moment [10], photoionization[11-13], UV-Vis absorbance[14-16], microwave[17] and

infrared[18] spectroscopy. Quinoline has also general astrophysical interest [19-21]. Nevertheless, few experimental negative ion gas phase studies exist. The compound negative ion resonance (CNIR) [22] of quinoline was reported and the gas phase lifetime[23] of the negative parent ion was determined, however, no experimentally measured electron affinity value for quinoline has been reported in the literature.

Here, we present the vibrationally-resolved anion photoelectron spectrum of quinoline$^-$ anion. From the spectrum we determined the adiabatic electron affinity to be 0.16 ± 0.05eV. This assignment is supported by our theoretical calculations and computationally simulated spectrum. The active vibrational frequencies observed compare favorably with previous experimentally measured vibrational modes of quinoline.

2.2 Methods

Experimental

Anion photoelectron spectroscopy is conducted by crossing a mass-selected beam of negative ions with a fixed-frequency photon beam and energy-analyzing the resultant photodetached electrons. The photodetachment process is governed by the relationship hν = EBE + EKE, where hν is the photon energy, EBE is the electron binding energy, i.e., the transition energy between the anion and a particular vibronic state of its neutral counterpart, and EKE is the electron kinetic energy. Negative ions of quinoline were formed in a biased (-500 V) supersonic expansion nozzle-ion source, where the quinoline sample was placed in a stagnation chamber, heated to 70 °C, and coexpanded with ~30 psig of argon gas through a 23 μm orifice into ~10^{-4} Torr vacuum. Negative ions were formed by injecting low energy electrons from a

more negatively biased, thoriated-iridium filament into the expanding jet, where a microplasma was formed in the presence of a weak external magnetic field. These anions were then extracted, collimated, and transferred into the flight tube of a 90° magnetic sector mass spectrometer with a mass resolution of ~400. The mass-selected anions of interest were then crossed with the intracavity laser beam of an argon ion laser, and the photodetached electrons were energy-analyzed in a hemispherical electron energy analyzer having a resolution of ~20 meV. The photoelectron spectrum reported here was recorded with 2.540 eV photons (488 nm), and it was calibrated against the photoelectron spectrum of the O^- anion[24]. It was also measured at lower resolution using our pulsed photoelectron magnetic bottle instrument.

Computational

Density functional theory (DFT) calculations of quinoline neutral and anion were performed with the Gaussian09[25] software package. Geometry optimizations, energy calculations and frequency analysis were all performed with the unrestricted wb97xd[26]functional and aug-cc-pVTZ[27-28] basis set. The highest occupied molecular orbital of the relaxed anion was generated in GaussView[29]. A simulated photoelectron spectrum was generated using the Franck-Condon method as implemented [30] in Gaussian09 using the default parameters which includes a convolution of the spectrum with Gaussian distributions with a 135 cm^{-1} half-width at half-maximum.

2.3 Results and Discussion

The photoelectron spectrum of quinoline anion, presented in Figure 1a, exhibits a vibrationally resolved profile. The observed transitions are centered at EBE 0.16 eV (peak A), 0.23 eV (peak B), 0.33 eV (peak C), and 0.52 eV (peak D). The lowest EBE transition in the spectrum is its origin-containing transition, i.e., the $\nu'=0 \leftarrow \nu''=0$ transition, and it defines the adiabatic electron affinity. Thus, $EA_a(C_9H_7N)$ was determined to be 0.16 eV ± 0.05 eV (Peak A). Our electronic structure calculations, including the zero-point energy, found quinoline to support a bound valence anion with an EA of 0.19 eV, which is in very good agreement with our experimentally measured value and the previous calculated semi-empirical value of 0.2eV[2]. Since the electron is added to a closed shell molecule, the electron affinity is expected to be small. There is scant evidence of vibrational hot bands in the spectrum, possibly because of anion autodetachment. The optimized geometries for both anion and neutral quinoline were calculated and found to be planar with very similar bond lengths between the structures (Figure 2a). The highest occupied molecular orbital (HOMO) structure for the quinoline anion is shown in Figure 2b, where the excess electron is delocalized in the π^* anti-bonding orbital. A computationally simulated photoelectron spectrum was generated and is also shown in Figure 1b. The profile of the calculated spectrum matches well compared to the experimentally measured photoelectron spectrum.

Since quinoline is a planar species belonging to the C_s point group, there are 45 vibrational modes that can be classified as even or odd, 31A′ and 14A″, respectively. The A′ modes will have the greatest Franck-Condon overlap and be active in a photoelectron spectrum.

The vibrational frequencies from Figure 1a were measured as the energy spacing between peak centers in the spectrum and are presented in Table2.1. Previous IR studies were considered to identify and assign the vibrational modes[18]. The vibrational frequency 565cm^{-1} (spacing between A and B) is assigned as vibrational mode ν_{29}, an in-plane ring distortion. The adjacent vibrational frequency (between A and C) at 1371 cm^{-1} is assigned as the vibrational modes ν_{14} and ν_{15} a C-C bond stretch. The spacing between A and D is 2904 cm^{-1} which corresponds to the C-H vibrational modes $\nu_{1\text{-}7}$. The calculated vibrational frequencies are close to the experimentally measured vibrational modes which is expected since the calculated simulated spectrum of quinoline is very similar to the experimentally measured spectrum (Table 1).

2.4 Summary

The molecule quinoline, displays a greater electrophilicty than its analog, naphthalene. Quinoline anion was formed by injecting low energy electrons into a supersonic expansion of the molecule seeded in argon and the anion photoelectron spectrum was recorded. A small but positive electron affinity of 0.16 eV was experimentally measured, indicating that quinoline supports a valence bound anion. Density functional theory calculations at the wb97xd /aug-cc-pVTZ level of theory found the electron affinity to be 0.19 eV. Both our experimental and theoretical results were in good agreement with those from previous studies.

References

[1] T. L. Kuni and H. Kuroda, Theoret. Chim. Acta (Berl.) 11, 97 (1968).

[2] J. M. Younkin, L. J. Smith and R. N. Compton, Theoret. Chim. Acta (Berl.) 41, 157 (1976).

[3] A. E. Ozel, Y. Buyukmurat and S. Akyuz, J. Mol. Struct. 565-566, 455 (2001).

[4] E. E. Ebenso, M. M. Kabanda, T. Arslan, M. Saracoglu, f. Kandemirli, L. C. Murulana, A. K. Singh, S. K. Shukla, B. Hammouti, K. F. Khaled, M. A. Quraishi, I. B. Obot and N. O. Eddy, Int. J. Electrochem. Sci. 7, 5643 (2012).

[5] L. Goodman and R. W. Harrell, J. Chem. Phys. 30, 1131 (1959).

[6] G. Favini, I. Vandoni and M. Simoneta, Theoret. Chim. Acta. (Berl.) 3, 45 (1965).

[7] K. Nishimoto, Theoret. Chim. Acta. (Berl.) 10, 65 (1968).

[8] R. D. Brown and B. A. W. Coller, Theoret. Chem. Acta. (Berl.) 7, 259 (1967).

[9] B. Tinland, Theoret. Chim. Acta. (Berl.) 8, 361(1967).

[10] A. D. Buckingham, J. Y. H. Chau, H. C. Freeman, R. J. W. Le Fevre, D. A. A. S. N. Rao and J. Tardif, J. Chem. Soc. 1405-1411 (1956).

[11] A. J. Yencha and M. A. ElSayed, J. Chem. Phys. 48, 3469 (1968).

[12] F. Brogli, E. Heilbronner and T. Kobayashi, Helv. Chim. Acta. 55, 274 (1972).

[13] W. Schafer and A. Schweig, Tetrahedron Lett. 39, 3743 (1973).

[14] J. P. Byrne and I. G. Ross, Austral. J. Chem. 24, 1107 (1971).

[15] N. Mataga, Y. Kaigu and M. Koizumi, Bull. Chem. Soc. Japan, 29, 373(1956).

[16] J. E.Purvis, J Chem. Soc. Trans. 97,1035 (1910).

[17] Z. Kisiel, O. Desyatnyk, L. Pszczolkowski, S. B. Charnley and P. Ehrenfreund, J. Mol. Spectrosc. 217, 115 (2003).

[18] S. C. Wait and J. C. McNerney, J. Mol. Spectrosc. 34, 56 (1970).

[19] P. G. Stoks and A. W. Schwartz, Geochim. Cosmochim. Ac. 46, 309 (1982).

[20] S. B. Charnley, Y.-J. Kuan, H.-C. Huang, O. Botta, H. M. Butner, N. Cox, D. Despois, P. Ehrenfreund, Z. Kisiel, Y.-Y. Lee, A. J. Markwick, Z. Peeters and S. D. Rodgers. Adv. Space Res. 36, 137 (2005).

[21] J. E. Elsila, M. R. Hammond, M. P. Bernstein, S. A. Sandford and R. N. Zare, Meteorit. Planet. Sci. 41, 785 (2006).

[22] M. N. Pisanias, L. G. Christophorous and J. G. Carter, Chem. Phys. Lett. 13, 433 (1972).

[23] A. Hadjiantonious, L. G. Christophorou and J. G. Carter, J. Chem. Soc., Faraday Trans. 2, 69, 1704 (1973).

[24] A. Joiner, R. H. Mohr and J. N. Yukich, Phys. Rev. A. 83, 035401 (2011).

[25] Gaussian 09, Revision A.2, M. J. Frisch, G. W. Trucks, H. B. Schlegel, G. E. Scuseria, M. A. Robb, J. R. Cheeseman, G. Scalmani, V. Barone, B. Mennucci, G. A. Petersson, H. Nakatsuji, M. Caricato, X. Li, H. P. Hratchian, A. F. Izmaylov, J. Bloino, G. Zheng, J. L. Sonnenberg, M. Hada, M. Ehara, K. Toyota, R. Fukuda, J. Hasegawa, M. Ishida, T. Nakajima, Y. Honda, O. Kitao, H. Nakai, T. Vreven, J. A. Montgomery, Jr., J. E. Peralta, F. Ogliaro, M. Bearpark, J. J. Heyd, E. Brothers, K. N. Kudin, V. N. Staroverov, R. Kobayashi, J. Normand, K. Raghavachari, A. Rendell, J. C. Burant, S. S. Iyengar, J. Tomasi, M. Cossi, N. Rega, J. M. Millam, M. Klene, J. E. Knox, J. B. Cross, V. Bakken, C. Adamo, J. Jaramillo, R. Gomperts, R. E. Stratmann, O. Yazyev, A. J. Austin, R. Cammi, C. Pomelli, J. W. Ochterski, R. L. Martin, K. Morokuma, V. G. Zakrzewski, G. A. Voth, P. Salvador, J. J. Dannenberg, S. Dapprich, A. D. Daniels, Ö. Farkas, J. B. Foresman, J. V. Ortiz, J. Cioslowski, and D. J. Fox.

[26] J.-D. Chai and M. Head-Gordon, Phys. Chem. Chem. Phys.10, 6615 (2008).

[27] D. E. Woon and T. H. Dunning, Jr. J. Chem. Phys. 90, 1007 (1989).

[28] D. E. Woon and T. H. Dunning, Jr. J. Chem. Phys. 98, 1358 (1993).

[29] GaussView, Version 5.0, R. Dennington, T. Keith and J. Millam, *Semichem Inc.*, Shawnee Mission, KS, 2009.

[30] F. Santoro, A. Lami, R. Improta, J. Bloino and V. Barone, J. Chem. Phys.128, 224311 (2008).

Table 2.1: Transition assignments for the photoelectron spectrum of quinoline compared with calculations from this studya and previously reported literature values

Experimental (this work)					Calculated (this work)		Reported values (from literature)	
Peak Location		Vibrational Spacing			Peak Location	Vibrational Mode	Experimental Vibrational Spacing[b]	Calculated Peak Location[c]
	(eV)	Δ	(eV)	(cm^{-1})	(eV)	(cm^{-1})	(cm^{-1})	(eV)
A	0.16				0.19			0.20
B	0.23	B-A	0.07	565	0.26	532, 535	522 (ν_{29})	
C	0.33	C-A	0.17	1371	0.37	1371	1392 (ν_{14}), 1371(ν_{15})	
D	0.52	D-A	0.36	2904	0.55	3161	3086(ν_1), 3056(ν_2), 3036(ν_3), 3014(ν_4), 3004(ν_5), 2979(ν_7)	

[a]Uncertainties are ± 0.05 eV or less.

[b]From ref [18].

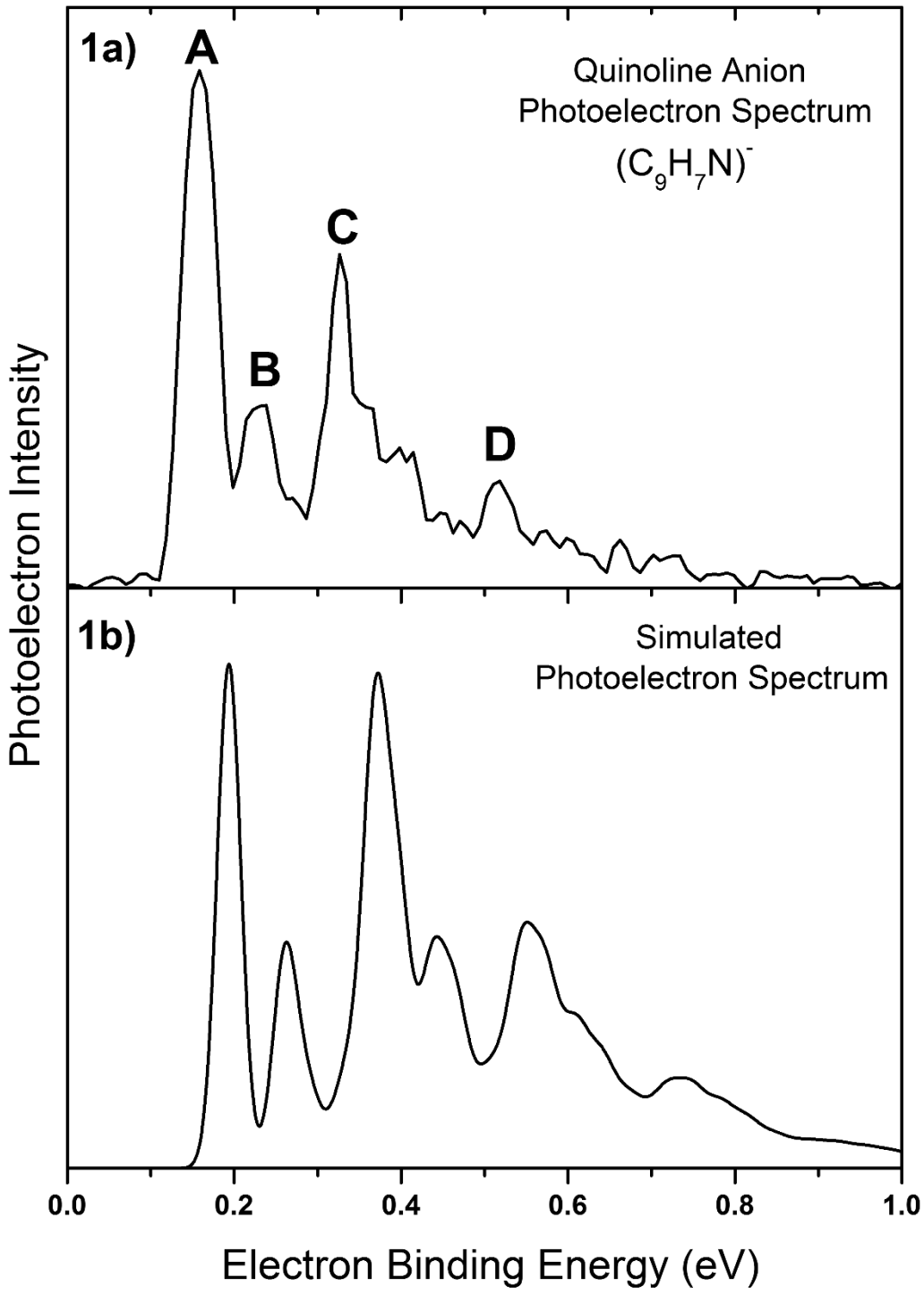

Figure 2.1: a) The measured photoelectron spectrum of the quinoline$^-$ anion recorded using 2.540 eV photons. b) The calculated Franck-Condon simulated photoelectron spectrum.

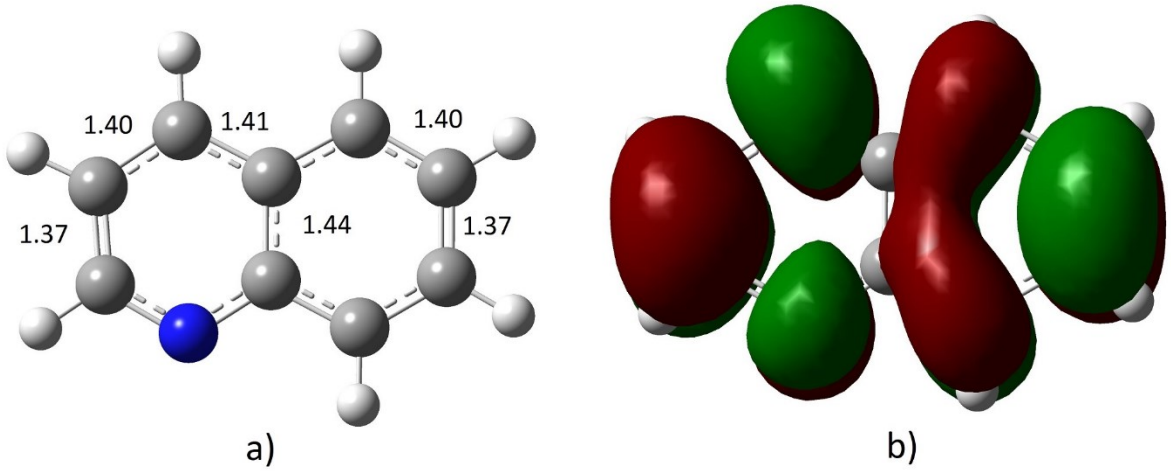

Figure 2.2: a) Optimized (wb97xd/aug-cc-pVTZ) structure of the quinoline$^-$ anion along with the critical bond lengths (Å). b) The highest occupied molecular orbital (HOMO) of the ground state of the anion.

Chapter 3. CO_2 Binding in the $(Quinoline\text{-}CO_2)^-$ Anionic Complex

Jacob Graham[1], Allyson Buytendyk[1], Yi Wang[1], Seong Keun Kim[2], and Kit H. Bowen, Jr. [1*]

[1]Department of Chemistry, Johns Hopkins University, Baltimore, MD 21218, USA

[2]Department of Chemistry, Seoul National University, Seoul, 151-747, Korea

3.1 Introduction

Carbon dioxide has long been known to bind weakly to certain amines[1], and more recently it has been found to bind to some metal organic frameworks (MOFs).[2] Carbon dioxide also forms gas-phase, anionic complexes with several atoms and molecules.[3-27] In the $[CO_2(H_2O)]^-$ anionic complex, for example, an intact CO_2^- sub-anion is stabilized by its interaction with water.[3,4] In seminal work, using a combination of mass spectrometry, photoelectron spectroscopy, and *ab initio* calculations, Kim and coworkers[5] found significant covalent character in the intermolecular bond between CO_2 and pyridine in the gas phase $(Pyridine\text{-}CO_2)^-$ anionic complex. Vibrational predissociation studies by Johnson and coworkers[6] confirmed its structure and the covalent bonding character inferred by Kim. In further studies with CO_2 and the heterocyclic nitrogen molecules: pyrazine, pyridazine, pyrimidine, triazine, and 2-aminopyridine, analogously bonded binary anionic complexes were also found.[7,8]

In all these cases, bonding took place between the carbon atom in CO_2 and a nitrogen atom in its heterocyclic molecular partner. From a Lewis acid-base perspective, the heterocycle's nitrogen atom, i.e., its lone electron pair, was the electron donor and CO_2 was the electron acceptor, both well-known properties of these constituents. As neutral adducts some degree of binding would have been expected, but with the addition of excess electrons, robust binary anionic complexes were formed. Kim referred to the process by which this occurs as "associative

electron attachment", i.e., where a chemical bond was formed due to electron attachment, even though there was no such bond in the corresponding neutral.[7] In each of the cases considered here, bond formation was likely due to delocalization of the excess electron over both the heterocycle's ring and the CO_2 moiety, i.e., over the entire molecular framework. This helps to rationalize why even though neither CO_2 nor any of its above-mentioned partners possess positive adiabatic electron affinities, together, they formed stable anionic complexes.

While covalent bonding character has been demonstrated for $(\text{N-Heterocycle-}CO_2)^-$ anionic complexes, carbon dioxide's binding energy there has not. Neither of the experimental techniques used to study them could have provided that information, and theoretical calculations were stymied by the necessity of dealing with molecules having negative adiabatic electron affinities. Quinoline, on the other hand, is different from the other N-heterocyclic molecules listed above in that it has a positive adiabatic electron affinity (0.16 eV).[28] This affords an opportunity to determine carbon dioxide's binding energy in the $(\text{Quinoline-}CO_2)^-$ anionic complex and by implication to estimate it in other $(\text{N-Heterocycle-}CO_2)^-$ anionic complexes as well. In the work presented here, we used a combination of mass spectrometry, anion photoelectron spectroscopy, and density functional calculations to study the $(\text{Quinoline-}CO_2)^-$ anionic complex and to identify a value for carbon dioxide's binding energy there.

3.2 Experimental and Computational Methods

Anion photoelectron spectroscopy is conducted by crossing a mass-selected beam of negative ions with a fixed-frequency photon beam and energy-analyzing the resultant photodetached electrons. The photodetachment process is governed by the relationship $h\nu = EBE + EKE$, where $h\nu$ is the photon energy, EBE is the electron binding energy, i.e., the transition

energy between the anion and a particular vibronic state of its neutral counterpart, and EKE is the electron kinetic energy.

Negative ions of quinoline were formed in a biased (-500 V) supersonic expansion nozzle-ion source, where the quinoline sample was placed in the source's stagnation chamber, heated to 70 °C, and co-expanded with ~2 atmospheres of argon gas through a 23 μm orifice into a vacuum maintained at 10^{-4} Torr. Simultaneously, CO_2 was admitted very near the nozzle on its vacuum side and allowed to mix with the jet. Negative ions were formed by injecting low energy electrons from an even more negatively-biased, thoriated-iridium filament into the expanding jet, where a micro-plasma was formed in the presence of a weak axial magnetic field. The resulting anions were then extracted, collimated, and transferred into the flight tube of a 90° magnetic sector mass spectrometer with a mass resolution of 400. Mass-selected anions of $(Quinoline\text{-}CO_2)^-$ were then crossed with the intra-cavity laser beam of an argon ion laser (~100 Watts), while photodetached electrons were energy-analyzed in a hemispherical electron energy analyzer having a resolution of 20 meV.[29] The photoelectron spectrum reported here was recorded with 2.540 eV photons (488 nm), and it was calibrated against the photoelectron spectrum of the O^- anion. An identical photoelectron spectrum of $(Quinoline\text{-}CO_2)^-$ was also observed in our lab using a pulsed anion photoelectron spectrometer that employed time-of-flight mass selection, a Nd:YAG laser, and a magnetic bottle electron energy analyzer.[30]

Density functional theory (DFT) calculations were conducted using the Gaussian 09 software package.[31] All calculations were performed using the wb97xd functional[32] and Aug-CC-pVTZ basis set.[33,34] Geometry optimizations were performed without symmetry constraints and were followed by vibrational frequency calculations to verify the identification of stationary points and to obtain zero point energies.

3.3 Results

The photoelectron spectrum of the (Quinoline-CO_2)$^-$ anionic complex is presented in Figure 1. This spectrum consists of a single broad band with an onset at EBE ~1.3 eV and an intensity maximum at EBE = 1.8 eV, the latter being its vertical detachment energy (VDE). Unlike the vibrationally-structured photoelectron spectrum of the quinoline molecular anion,[28] no vibrational features were resolved in the photoelectron spectrum of the (Quinoline-CO_2)$^-$ anionic complex.

Figure 2 presents the optimized geometries that we calculated for both the (Quinoline-CO_2)$^-$ anionic complex (Fig. 2A) and the Quinoline-CO_2 neutral complex (Fig. 2B). As can be seen in Fig. 2A, the C-N bond length in the (Quinoline-CO_2)$^-$ anionic complex is 1.55 Å and its CO_2 moiety is bent by 132^0. By comparison, the C-N bond distance in the Quinoline-CO_2 neutral complex is 2.83 Å. These structural parameters are quite similar to those of (Pyridine-CO_2)$^-$ and (Pryridine-CO_2). Kim[5] and Johnson[6] calculated the C-N bond length in the (Pyridine-CO_2)$^-$ anionic complex to be 1.46 Å and 1.52 Å, respectively, while Leopold[35] measured the C-N bond distance in the Pyridine-CO_2 neutral complex to be 2.798 Å. Furthermore, based on a Natural Population Analysis (NPA), we found the negative charge on the quinoline moiety to be 0.41*e,* while that on the CO_2 moiety is 0.59*e*. Even though the excess negative charge is delocalized over the entire anionic complex, it is somewhat more localized on the CO_2 moiety than on the quinoline moiety. Figure 3 presents the highest occupied molecular orbital (HOMO) of the (Quinoline-CO_2)$^-$ anionic complex. While both the HOMO and NPA approaches indicate electron delocalization over the whole complex, they are mapping different aspects of excess electron density.

The energy difference between the (Quinoline-CO_2)$^-$ anionic complex in its relaxed geometry and the Quinoline-CO_2 neutral complex in that same geometry is the VDE value. Our calculated VDE of 1.77 eV is in very good agreement with the experimentally observed value of 1.8 eV. We also calculated the zero-point corrected, adiabatic electron affinity (EA) of Quinoline-CO_2 and found it to be 0.67 eV. However, due to the geometry difference between the relaxed structure of the anionic complex (Fig. 2A) and that of its neutral counterpart (Fig. 2B), it would not be surprising if Franck-Condon overlap between the two were to be insufficient for the origin transition to be observed in the experimental spectrum. That appears to be the case, since no significant features were seen in the spectrum in the vicinity of EBE = 0.67 eV. Thus, the EA value of the Quinoline-CO_2 complex could not be determined from the photoelectron spectrum alone.

Additionally, the zero-point corrected adiabatic electron affinity of quinoline itself was calculated to be 0.19 eV, compared with our experimental value of 0.16 eV.[28] Since the latter value derives from a straightforward assignment of our vibrationally-structured photoelectron spectrum of the quinolone molecular anion and is thus probably quite accurate, the 0.03 eV discrepancy between theory and experiment is probably a measure of the accuracy of our calculations. Relevant values are summarized in Table I.

3.4 Discussion

How strongly is CO_2 bound in the (Quinoline-CO_2)$^-$ anionic complex? Initially, we had hoped to determine this from the thermochemical relationship,

$$D_0\,(\text{Quinoline-}CO_2)^- = \text{EA}\,(\text{Quinoline-}CO_2) - \text{EA}\,(\text{Quinoline}) + D_0\,(\text{Quinoline-}CO_2) \quad (1)$$

using our experimental values for EA (Quinoline-CO_2) and EA (Quinoline) and a calculated value for D_0 (Quinoline-CO_2), which was in any case expected to be relatively small. This approach, however, could not be used when the origin transition failed to appear in the photoelectron spectrum of the (Quinoline-CO_2)$^-$ anionic complex, due to a lack of Franck-Condon overlap.

We then turned to a computational approach. Theoretical attempts to calculate the binding energy of CO_2 in the earlier mentioned (N-Heterocycle-CO_2)$^-$ anionic complexes would have been stymied by the difficulty of dealing with molecules having negative adiabatic electron affinities, i.e., both CO_2 and the N-heterocyclic molecules mentioned above. Quinoline, on the other hand, possesses a positive adiabatic electron affinity, and that made it possible for us to calculate the absolute energy of its anion. The dissociation energy of the (Quinoline-CO_2)$^-$ anionic complex, D_0 (Quinoline-CO_2)$^-$, breaking into the quinoline molecular anion, (Quinoline)$^-$ and CO_2, is given by:

$$D_0\,[(\text{Quinoline-}CO_2)^-] = E\,[(\text{Quinoline})^-] + E\,[CO_2] - E\,[(\text{Quinoline-}CO_2)^-] \qquad (2)$$

where E [M] refers to the calculated absolute energy of species, M, in its relaxed geometry and with its zero point energy included. By this approach, D_0 [(Quinoline-CO_2)$^-$] was found to be 0.64 eV.

Likewise, the dissociation energy of the (Quinoline-CO_2) neutral complex, D_0 (Quinoline-CO_2), breaking into the neutral quinoline molecule and CO_2, is given by:

$$D_0\,[(\text{Quinoline-}CO_2)] = E\,[\text{Quinoline}] + E\,[CO_2] - E\,[(\text{Quinoline-}CO_2)] \qquad (3)$$

where again E [M] refers to the calculated absolute energy of species, M, in its relaxed geometry and with its zero point energy included. In this way, D_0 [(Quinoline-CO_2)] was found to be 0.16 eV. By comparison, the binding energy of the Pyridine-CO_2 neutral complex has been calculated to be 0.10 - 0.20 eV.[36] Lastly, notice that our computed values are consistent, i.e., eqn. (1) balances when they are inserted into it. Also, the fact that our calculated and measured values for EA (Quinoline), i.e., 0.19 eV and 0.16 eV, respectively, are so close to one another provides reassurance in the validity of the calculations.

Our results indicate that carbon dioxide is bound by 0.64 eV in the (Quinoline-CO_2)$^-$ anionic complex. This suggests that the earlier discussed (N-Heterocycle-CO_2)$^-$ anionic complexes also have comparable CO_2 binding energies. Following Kim's and Johnson's conclusions that the (Pyridine-CO_2)$^-$ anionic complex exhibits significant covalent bonding character, it seems likely that the (Quinoline-CO_2)$^-$ anionic complex does too. Still, 0.64 eV is well below the bond strength of a most covalent bonds. On the other hand, it is much stronger than a van der Waals bond and also stronger than most hydrogen bonds. A binding energy of 0.64 eV lies in an intermediate range, i.e., along a continuum of bond strengths between those of van der Waals and chemical interactions. It fits best among the interaction strengths of Lewis acid-base pairs (adducts). For neutral-neutral complexes, these span binding energies form ~0.2 eV to significantly over an electron volt.[37,38] For binary complexes with net negative charges, however, there are few signposts to guide us within the context of Lewis acid-base pairs. Perhaps, the best we have are $O_2^-(CO_2)$ and $NO^-(CO_2)$, which could be thought of as Lewis acid-base pairs and whose binding energies have been measured[16] or calculated[39] to be 0.82 eV and 0.9 eV, respectively. Like (Quinoline-CO_2)$^-$, their non-CO_2 moieties form stable negative ions, but unlike (Quinoline-CO_2)$^-$, neither $O_2^-(CO_2)$ nor $NO^-(CO_2)$ can significantly delocalize their excess

charges. In fact, both $O_2^-(CO_2)$ and $NO^-(CO_2)$ might better be considered to be ion-molecule complexes. By contrast, because all the (N-Heterocycle-CO_2)$^-$ anionic complexes discussed here owe their stabilities to their ability to delocalize their excess charges, they belong to a distinct class of negatively-charged complexes.

For CO_2, taking on partial negative charge means that it must bend to a corresponding degree and correspondingly bending presumes the acquisition of negative charge density. They are two side of the same coin; for CO_2, bending and accepting negative charge are synonymous. This relationship lies at the heart of CO_2 activation, and it is much in evidence in the binding of CO_2 within (N-Heterocycle-CO_2)$^-$ anionic complexes.

Acknowledgements

We thank Alex Boldyrev and Ken Leopold for valuable correspondence on this topic. This research was supported in part by the U.S. Department of Energy, Office of Basic Energy Sciences, Division of Chemical Sciences, Geosciences and Biosciences under Award DE-FG02-12ER16362. This material is also based in part on work supported by the U. S. National Science Foundation under grant number CHE-1360692. This work was also supported in part by the Global Frontier R&D Program of the Center for Multi-Scale Energy Systems funded by the National Research Foundation under grant number, NRF-2014M3A6A7060583 (SKK).

References

1. G. Astarita, *Chem. Engr, Sci,* 16, 202-207 (1961).

2. K. Sumida, D. L. Rogow, J.A. Mason, T. M. McDonald, E. D. Bloch, Z. R. Herm, T-H. Bae, and J. R. Long, *Chem. Rev*. 112, 724-781 (2012).

3. C. E. Klots, *J. Chem. Phys.* 71, 4172 (1979).

4. T. Tsukuda and T. Nagata, *J. Phys, Chem. A* 107, 8476 (2003).

5. S. Y. Han, I. Chu, J. H. Kim, J. K. Song, and S. K. Kim, *J. Chem. Phys*. 113, 596 (2000).

6. M. Z. Kamrath, R. A. Relph, and M. A. Johnson, *J. Am. Chem. Soc.* 132, 15508 (2010).

7. S. H. Lee, N. Kim, D. G. Ha, and S. K. Kim, *J. Am. Chem. Soc*. 130, 16241 (2008).

8. N. Kim, *Bull. Korean Chem. Soc*. 34, 2247 (2013).

9. M. J. DeLuca, B. Niu, and M. A. Johnson, *J. Chem. Phys*. 88, 5857 (1988).

10. S. H. Fleischman and K. D. Jordan, *J. Phys. Chem.* 91, 1300 (1987).

11. T. Tsukuda, M. A. Johnson, and T. Nagata, *Chem. Phys. Lett.* 268, 429 (1997).

12. J. W. Shin, N. I. Hammer, M. A. Johnson, H. Schneider, A. Glöβ, and J.M. Weber, *J. Phys. Chem. A* 109, 3146 (2005).

13. D. W. Arnold, S. E. Bradforth, E. H. Kim, D. M. Neumark, *J. Chem. Phys.* 102, 3493 (1995).

14. H. Schneider, A. D. Boese, and J. M. Weber, *J. Chem. Phys.* 123, 074316 (2005).

15. A. Muraoka, Y. Inokuchi, N. I. Hammer, J,-W, Shin, M. A. Johnson, and T. Nagata, *J. Phys, Chem. A* 113, 8942 (2009).

16. K. Hiraoka and S. Yamabe, *J. Chem. Phys.* 97, 643 (1992).

17. K. Sudoh, Y. Matsuyama, A. Muraoka, R. Nakanishi, and T. Nagata, *Chem. Phys, Lett.* 433 10-14 (2006).

18. T. Sanford, S.-Y. Han, M. A. Thompson, R. Parson, and W.C. Lineberger, *J. Chem. Phys*. 122, 054307 (2005).

19. J. M. Weber, *Int. Rev. Phys. Chem*. 33, 489 (2014).

20. A. D. Boese, H. Schneider, A. N. Glöß, and J. M. Weber, *J. Chem. Phys.* 122, 154301 (2005).

21. B. J. Knurr and J. M. Weber, *J. Am. Chem. Soc.* 134, 18804 (2012).

22. B. J. Knurr and J. M. Weber, *J. Phys. Chem. A* 118, 4056 (2014).

23. B. J. Knurr and J. M. Weber, *J. Phys. Chem. A* 118, 10246 (2014).

24. B. J. Knurr and J. M. Weber, *J. Phys. Chem. A* 118, 8753 (2014).

25. R,F. Hoeckebdorf, K. Fischmann, Q. Hao, C. v.d. Linde, O. P, Balaj, C-K. Siu, and M. K. Beyer, *Intern. J. Mass Spectro*. 354, 175 (2013).

26. A. Akhgarnusch, R. F. Hoeckebdorf, Q. Hao, K. P. Jaeger, C-K. Siu, and M. K. Beyer, *Angew, Chem. Int. Ed.* 53, 9327 (2013).

27. A. Akhgarnusch and M. K. Beyer, *Intern. J. Mass Spectro*. 365, 295 (2014).

28. A. M. Buytendyk, Y. Wang, J. D. Graham, A. K. Kandalam, B. Kiran and K. H. Bowen, *Molecular Physics*. (2015) [DOI: 10.1080/00268976.2014.1003261].

29. J. V. Coe, J. T. Snodgrass, C. B. Freidhoff, K. M. McHugh, and K. H. Bowen, *J. Chem. Phys.,* 87, 4302-4309 (1987).

30. D. Wang, J.D. Graham, A.M. Buytendyk, and K.H. Bowen, *J. Chem. Phys*., 135, 164308 (2011).

31. Gaussian 09, Revision A.2, M. J. Frisch, G. W. Trucks, H. B. Schlegel, G. E. Scuseria, M. A. Robb, J. R. Cheeseman, G. Scalmani, V. Barone, B. Mennucci, G. A. Petersson, H. Nakatsuji, M. Caricato, X. Li, H. P. Hratchian, A. F. Izmaylov, J. Bloino, G. Zheng, J. L. Sonnenberg, M. Hada, M. Ehara, K. Toyota, R. Fukuda, J. Hasegawa, M. Ishida, T. Nakajima, Y. Honda, O. Kitao, H. Nakai, T. Vreven, J. A. Montgomery, Jr., J. E. Peralta, F. Ogliaro, M. Bearpark, J. J. Heyd, E. Brothers, K. N. Kudin, V. N. Staroverov, R. Kobayashi, J. Normand, K. Raghavachari, A. Rendell, J. C. Burant, S. S. Iyengar, J. Tomasi, M. Cossi, N. Rega, J. M. Millam, M. Klene, J. E. Knox, J. B. Cross, V. Bakken, C. Adamo, J. Jaramillo, R. Gomperts, R. E. Stratmann, O. Yazyev, A. J. Austin, R. Cammi, C. Pomelli, J. W. Ochterski, R. L. Martin, K. Morokuma, V. G. Zakrzewski, G. A. Voth, P. Salvador, J. J. Dannenberg, S. Dapprich, A. D. Daniels, Ö. Farkas, J. B. Foresman, J. V. Ortiz, J. Cioslowski, and D. J. Fox, Gaussian, Inc., Wallingford CT, 2009.

32. J.-D. Chai and M. Head-Gordon, *Phys. Chem. Chem. Phys*., 10, 6615-20 (2008).

33. D. E. Woon and T. H. Dunning, Jr. *J. Chem. Phys.* 90, 1007 (1989).

34. D. E. Woon and T. H. Dunning, Jr. *J. Chem. Phys.* 98, 1358 (1993).

35. J. L. Doran B. Hon and K. R. Leopold, *J. Mol. Struct.* 1019, 191 (2012).

36. K. D. Vogiatzis, A. M.avrandonakis, W. Klopper, G. E. Froudakis, *ChemPhysChem.* 10, 374 (2009).

37. K. R. Leopold, *Adv. Mol. Struct. Res.* 2, 103 (1996).

38. K. R. Leopold, M. Canagaratna, and J. A. Philips, *Accts. Chem. Res.* 30, 57 (1997).

39. M. Zhou, L. Zhang, and Q. Qin, *J. Am Chem. Soc.* 122, 4483 (2000).

	Exp EA	Calc EA	Calc EA with ZPE	Exp VDE	Calc VDE
Quinoline	0.16[a]	0.05[a]	0.19[a]	--------	---------
Quinoline-CO_2	<1.3	0.64	0.67	1.8	1.77

(a) ref. 28

Table 3.1. Experimental and Calculated Electron Affinities and Vertical Detachment Energies for Quinoline and Quinoline-CO_2 Complexes**.**

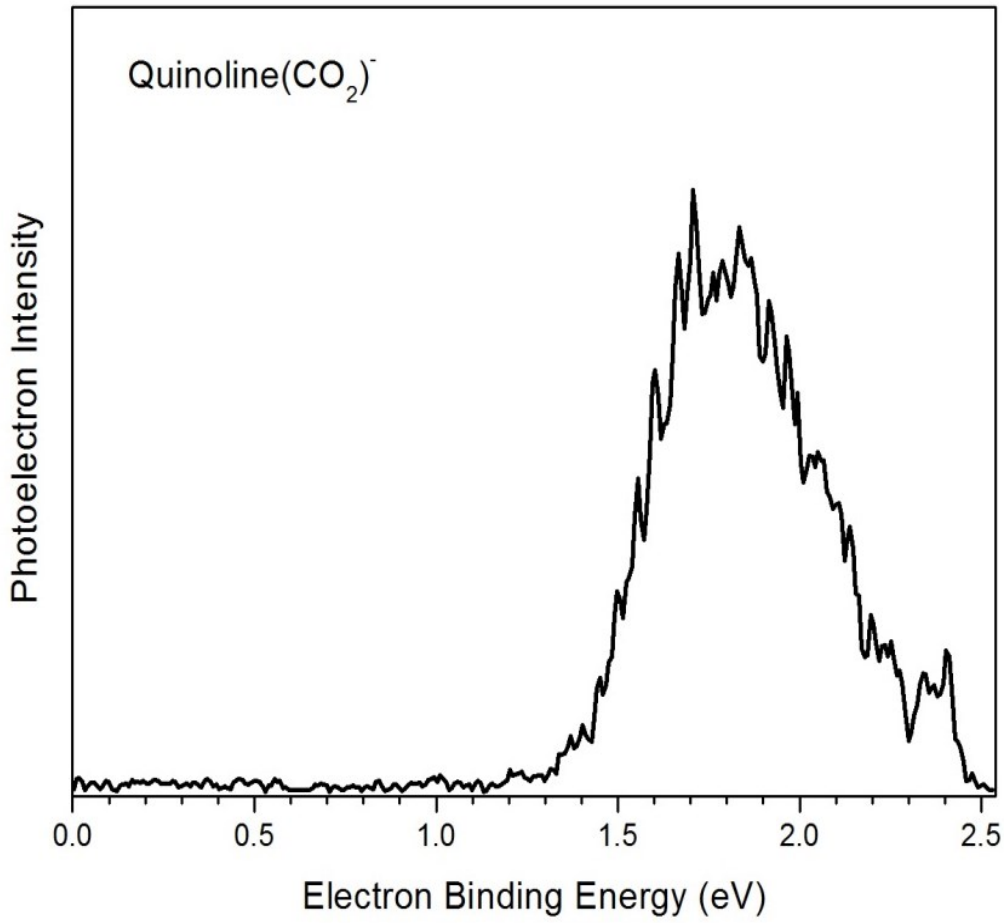

Figure 3.1. The anion photoelectron spectrum of the (Quinoline-CO_2)$^-$ anionic complex recorded with 488 nm photons.

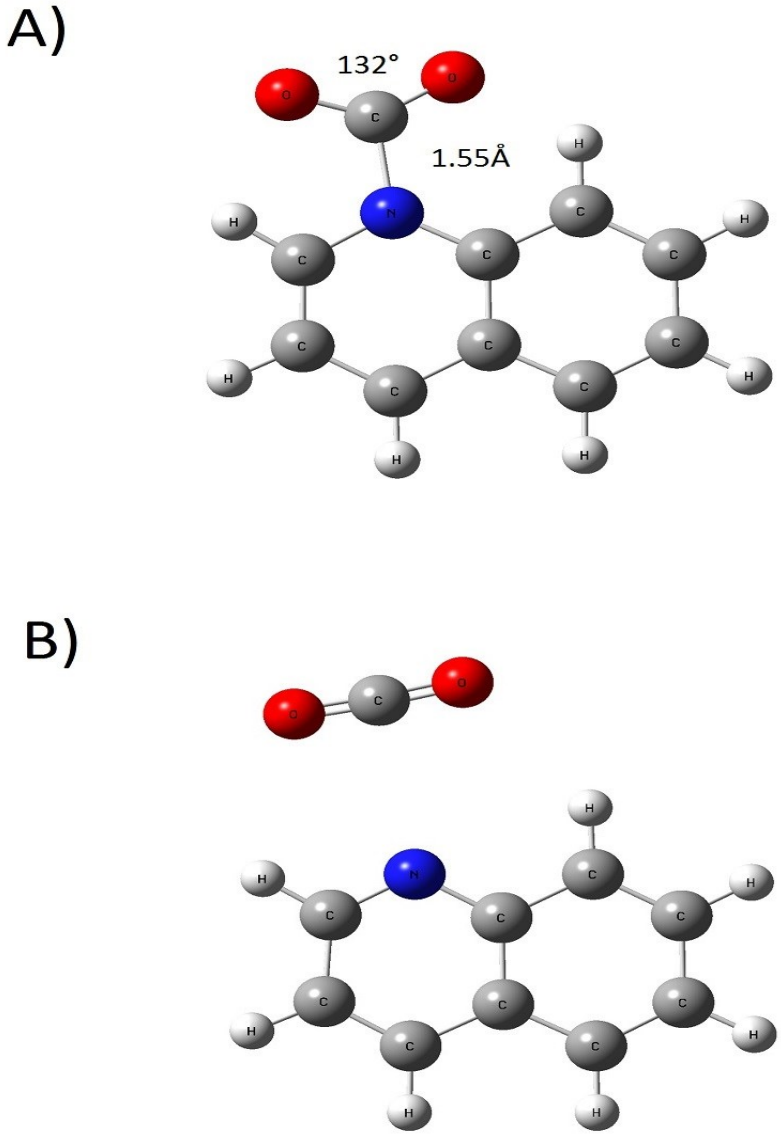

Figure 3.2. Relaxed geometries of (A) the (Quinoline-CO_2)$^-$ anionic complex and (B) the Quinoline-CO_2 neutral complex.

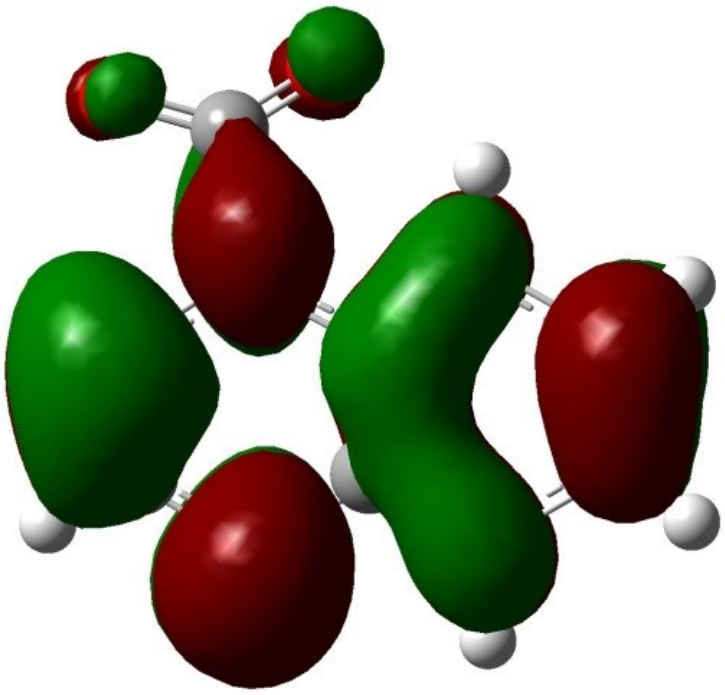

Figure 3.3. The highest occupied molecular orbital (HOMO) of the (Quinoline-CO_2)$^-$ anionic complex.

Chapter.4 Negative ion properties of trans-2,2',6,6'-tetrafluoro-azobenzene: Experiment and Theory

Mohammadreza Rezaee,[1] Yi Wang,[3] Xinxing Zhang,[3] Gaoxiang Liu,[3] Kit Bowen,[3] Andrew M. Bayer,[2] Michel D. Best[2] and Robert N. Compton,[1,2]

[1] Department of Physics, University of Tennessee, Knoxville, Tennessee 37996, USA

[2] Departments of Chemistry, University of Tennessee, Knoxville, Tennessee 37996, USA

[3] Departments of Chemistry, John Hopkins University, Baltimore, Maryland 21218, USA

Abstract

Chemical bonding and the electronic structure of the trans-2,2',6,6'-tetrafluoro-azobenzene negative ion have been studied by collision induced dissociation (CID) as well as photodetachment photoelectron spectroscopy (PD-PES) and the experimental results were compared with ab initio calculations. The parent anion was prepared by atmospheric pressure chemical ionization (APCI) for the collision induced dissociation experiment and through thermal electron attachment in the PES experiments. The adiabatic electron affinity of trans-2,2',6,6'-tetrafluoro-azobenzene is measured to be 1.3 ± 0.1 eV and the vertical detachment energy is 1.78 eV. The calculated adiabatic and vertical electron affinities using wB97XD/6-311++G(d,p) calculation are 1.5 eV and 1.0 eV respectively and the vertical detachment energy is 1.74 eV and in close agreement with the experimental results. Energy resolved collision induced dissociation of the parent anion resulted in 1.88 ± 0.2 eV bond dissociation energy for the collision process yielding $[\boldsymbol{C_6H_3F_2}]^-$ and $\boldsymbol{C_6H_3F_2N_2}$. *Ab initio* calculations result in a dissociation energy of ~1.8 eV at room temperature. Two other product ions include $[\boldsymbol{C_6H_2F}]^-$

and $[\boldsymbol{C_6H}]^-$ which on energetic arguments are believed to be due to collisional losses of HF from $[\boldsymbol{C_6H_3F_2}]^-$ The occurrence of $[\boldsymbol{C_6H}]^-$ is of particular interest since it is the first anion to be observed in the interstellar medium.

4.1 Introduction

Azobenzene (diphenyldiazene) consist of two benzene rings connected by single C-N bonds to N=N and exists as trans- and cis- isomers exhibiting an orange-red color. First described by the German chemist Eilhard Mitscherlich[1] in 1834 azobenzene and its derivatives include more than 70% of commercial dyes owing to their vibrant, chemically tunable colors, and extreme durability even upon continuous irradiation.[2] Azobenezene and its derivatives are photo-responsive and can mechanically change its cis/trans geometry upon radiation making them excellent candidates for photo-switching. Photochromic switches that are able to quickly transmit information have attracted a growing interest because of the potential applicability of such systems as active data storage and communication elements in many devices, such as optical systems for opto-electronics, holographic materials and multi-color displays during the last few decades.[3] The cis-form of azobenzene has been known since 1937 when Hartley[4] performed photometric studies of azobenzene and observed that the solubility of azobenzene changed after being irradiated with sunlight. The photo-isomerization change from trans- to the thermodynamically less stable cis- form occurs quickly using UV light (300-400 nm) and the backward reaction occurs using light (visible blue light >400 nm) or thermally on the timescale of minutes.[5] Azobenzene and its derivatives have attracted much interest because of the large-amplitude structural changes between their cis- and trans- isomers, the reversibility of their transformations and the high photo-stabilities guarantee large numbers of switching cycles.[6] As such the azobenzene family represents promising candidates in future molecular switches, light harvesting materials, photonic devices, and photo-controllable materials.[7] They also have remarkable biological applications such as remotely controlling cellular functions.[8] Designing an azobenzene amino acid opens the possibilities for biological incorporation of photo-switches *in situ*.[9] Azobenzene doped polymers and liquid crystals have fascinating potential applications in

biology, photonic, biophysics, nonlinear optics and their diverse possible technological applications have been intensely investigated.[10-12] Fluorinated azobenzene derivatives have been recently synthesized. Bushuyev et al.[13] studied fluorinated azobenzene and showed that these solids can directly convert visible light into mechanical motion with high isomerization efficiency and chemical stability under multiple isomerization cycles. Functionalizing azobenzene eliminates the need for employing UV light for photo-switching making it more thermally stable and favorable in bio-applications. Recently Gan et al.[14] studied a series of fluorinated azobenzene esters and found that trans–cis isomerization occurs after 4 minutes and cis–trans isomerization occurred after 22 hours under the same conditions.

Figure 1 illustrates the cis and trans forms of 2,2',6,6'-tetrafluoro- azobenzene optimized at the B3LYP level of theory with a 6-311++G(d,p) basis set. Calculations using B3LYP level of theory with 6-311++G(d,p) basis set results in a 0.29 Debye dipole moment for trans 2,2',6,6' tetrafluoro-azobenzene and 5.45 Debye for the cis-form. Notice that the trans-isomer is slightly twisted and is not planner which is the origin of the small dipole moment. Trans- azobenzene is a planer molecule with zero dipole moment. The trans- 2,2',6,6' tetrafluoro-azobenzene is 0.36 eV lower in the ground state electronic energy in compare to the cis- isomer.

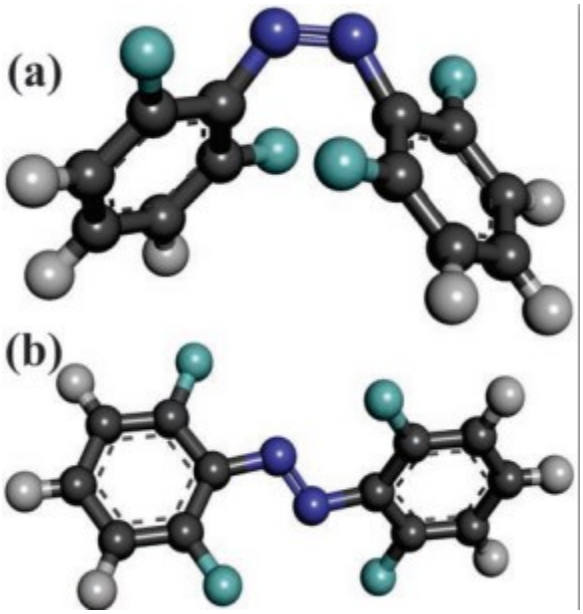

Figure.4.1 Optimized structure of 2,2',6,6'-tetrafluoro-azobenzene negative ion. (a) cis isomer (b) trans isomer. Optimization has been done using B3LYP level of theory with 6-311++G(d,p) basis set. Gaussian 09 output results have been visualized using Discovery studio 4.0 visualizer.

4.2 Methods

A. Synthesis of 2,2',6,6'-tetrafluoro-azobenzene

2,6-Difluoroaniline (662 µL, 1 g, 7.745 mmol) was dissolved in 40 mL of dichloromethane. Then using a mortar and pester, equal weight iron(II) sulphate heptahydrate and potassium permanganate (8 g total) were ground together and added into the flask. The reaction was heated to 40° C and proceed as shown.

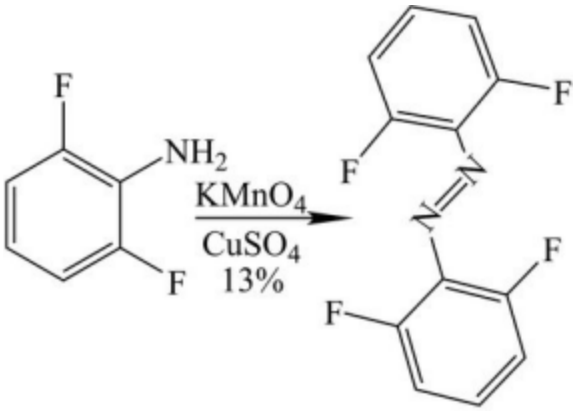

Figure. 4.2. The synthesis mechanism of 2,2',6,6'-tetrafluoro-azobenzene.

The following day the reaction was filtered through Celite and washed with dichloromethane. Column chromatography with 50% dichloromethane in hexanes, then dichloromethane gave product 2,2',6,6'-tetrafluoro-azobenzene (113 mg, 11%). ^{1}H NMR (300 MHz, $CDCl_3$) δ: 7.45-7.28 (m, 2H), 7.13-6.98 (m, 4H). ^{13}C NMR (75 MHz, $CDCl_3$) δ: 157.28 (d, J = 4.1 Hz), 153.82 (d, J =4.2 Hz), 131.48 (t, *J*=10.5 Hz), 112.60 (dd, *J*=20.7, 3.4 Hz). 19F (282 MHz, $CDCl_3$) δ: -124.94, referenced to 2,2,2-trifluoroethanol as an external standard. (There is a minor peak due to a partial existence of the Z isomer of the compound.) HRMS-DART: $[M]^-$, calculated for $C_{12}H_6F_4N_2$, 254.0467, found 254.0467.

B. Photodetachment photoelectron spectroscopy (PD-PES)

Anion photoelectron spectroscopy is conducted by crossing a mass-selected beam of negative ions with a fixed-frequency photon beam and energy-analyzing the resultant photodetached electrons. It is governed by the energy-conserving relationship, hν = EBE + EKE, where hν is the photon energy, EBE is the electron binding (transition) energy, and EKE is the electron kinetic energy. Our anion photoelectron spectrometer, which has been described previously,[15] consists of a laser vaporization anion source, a linear time-of-flight mass analyzer/selector, a pulsed Nd:YAG photodetachment laser (355 nm), and a magnetic bottle

electron energy analyzer/selector, a pulsed Nd:YAG photodetachment laser (355 nm), and a magnetic bottle electron energy analyzer. Photoelectron spectra were calibrated against the well-known photoelectron spectrum of Cu^-[16] Parent anions of tetrafluoro-azobenzene were generated in a photoemission source. Briefly, tetrafluoro-azobenzene sample powder was put into an oven and slightly heated to 30 °C, the vaporized molecules were then extracted by a plume of helium gas from a pulsed gas valve (backing pressure of ~150 psi). Just outside of the orifice of the oven, low energy electrons were produced by ablating a rotating and translating a Cu rod with a pulsed Nd:YAG laser beam operating at a wavelength of 532 nm. Negatively charged anions were then extracted into the spectrometer prior to mass selection and photodetachment.

C. Collision induced dissociation (CID):

Collision induced dissociation (CID) experiments are effective analytical methods based on mass spectroscopy to obtain important information about the thermochemical properties of ions. Combined with quantum chemistry computations CID experiments can be an accurate source of information in gas phase thermochemistry. Analysis of the energy dependence of the cross sections for collision-induced dissociation reactions has permitted the determination of quantitative thermodynamic information for a variety of ionized molecules.[17] Collision induced dissociation main strengths are the relatively direct manner of obtaining bond energies from dissociation thresholds, its broad dynamic range, and its ability to treat a diverse set of chemical species.[18] The CID experiments were carried out using an AB Sciex QSTAR Elite Hybrid LC/MS/MS apparatus which is a hybrid quadruple/time-of-flight mass spectrometer equipped with an atmospheric pressure chemical ionization (APCI) ion source. Negative ions are generated under atmospheric pressure conditions at high temperature, 573 K, using a corona

discharge. Low energy electron attachment to the molecule is followed by collisional stabilization in a bath gas. Anions are introduced to the instrument using nitrogen as the curtain gas. A major source of uncertainty here is the fact that the internal energies of the anions are not well characterized. A schematic of the QSTAR Elite Hybrid LC/MS/MS and the general method employed has been presented recently by Smith et al.[19] in study of negative ions of p-nitroaniline. The sample is dissolved in methanol as a dilute solution having 2 μg/ml concentration and injected to the instrument with 2 μL/min rate. Negative ions are produced in the discharge region by low energy electron attachment followed by collisional vibrational relaxation to approximately the nebulizer bath temperature. The parent ion of mass m/z = 254 was transmitted through the first quadrupole mass spectrometer and injected into the collision cell. Argon was used as the neutral target gas and the collision induced dissociation experiment has been performed with 22, 33 and 53 micro Torr pressure in the collision cell in order to investigate the single collision criteria. By extrapolating the cross sections obtained for different pressures, one can find the cross section for ideal zero pressure conditions. The collision cell is 20.9 cm long and is at room temperature. The laboratory frame collision energy was varied from 0 eV to 22 eV in increments of 0.5 eV and data were recorded for one minute at each energy point. Analysis of the recorded mass spectrum was performed by using the Analyst® QS 2.0 software package. To convert the data from an instrument dependent ion intensity signal in an energy resolved CID experiment and extract the threshold energy E_0 many factors such as the transition state of the reaction and the finite temperature of the ions and the collision cell must be considered. Converting the line intensities to cross sections has been performed using the following relationship:[20]

$$\boldsymbol{I_R = \left(I_R + \Sigma I_p\right) e^{-\sigma_{tot} nl}} \qquad (1)$$

where I_R is the parent ion intensity, I_P is the intensity of each product ion, σ_{tot} is the total cross section, l is the effective collision cell length and n is the density of particles in the collision cell which is related to the pressure and temperature of the neutrals, argon atoms, in the collision cell as $\boldsymbol{n} = \frac{\boldsymbol{P}}{\boldsymbol{k_B T}}$ P and T in this equation are the collision gas pressure and temperature and k_B is the Boltzmann constant.[21] This is valid only if there is no ion lost in the collision cell or in the path from the collision cell to the detector. There are several uncertainties in this regards. For example, there is an entrance and an exit to the cell which are connected to the turbo pumps resulting in a pressure profile along the collision cell length. Also, if the thin target approximation is valid, i.e. $\boldsymbol{nl\sigma_{tot}} \ll \mathbf{1}$, then the above equation can be simplified to:

$$\boldsymbol{\sigma_{tot}} = \frac{\sum \boldsymbol{I_P}}{\boldsymbol{nl}\,(\boldsymbol{I_R} + \sum \boldsymbol{I_P})} \tag{2}$$

We used the original form for the sake of accuracy. After obtaining the total cross section we can convert it to obtain a cross section for each of the product ions using:

$$\boldsymbol{\sigma_P} = \boldsymbol{\sigma_{tot}} \left(\frac{\boldsymbol{I_P}}{\sum \boldsymbol{I_P}} \right) \tag{3}$$

The center-of-mass energy (energy available for the reaction) is obtained from:

$$\boldsymbol{E_{CM}} = \boldsymbol{E_{lab}} \frac{\boldsymbol{m_{Ar}}}{(\boldsymbol{m_{Ar}} + \boldsymbol{m_p})} \tag{4}$$

where m_{Ar} and m_p are the mass of an Argon atom and the parent negative ion, respectively. To deconvolute the physical threshold energy from the experimental cross section data we utilized the so-called L-CID code developed by Bach et al.[22] at the Laboratory of Organic Chemistry ETH Zürich. Since this is a relatively new method, a brief description is necessary. Using L-CID is more convenient than other conventional methods since it only uses a single effective frequency with a new model for the density-of-states function and eliminates the need to explicitly calculate the frequencies for the parent ion and the transition state. Instead of conventional Marquardt-Levenburg least-squares routines, L-CID utilizes a Monte Carlo simulation and a sophisticated genetic algorithm to fit the data. L-CID uses a physical method to take into account the electrostatic potential for the two collision partners and properly consider the centrifugal barrier which is the direct result of the conservation of angular momentum. Input for L-CID requires the number of degrees of freedom, the looseness or tightness of the transition, number of free rotors, mass and polarizability of the target gas, experimental full width at half maximum (FWHM) of the kinetic ion energy distribution and the cross section data as a function of the energy in the center of mass or the laboratory frame.

Computations

Quantum mechanical methods, especially *ab initio* approaches have been widely used for computational thermochemistry and predicting properties of molecules and ions. The field of computational thermochemistry has matured to the point that for small molecules it is possible to predict reaction enthalpies to accuracies rivalling the best experiments.[23] Here we used several density functional methods as well as high accuracy CBS-QB3 method to calculate the bond dissociation energies along with other properties such as adiabatic and vertical electron affinity

and the vertical detachment energy. Ground state properties of the negative ion, the neutral molecule and the transition state geometry optimizations and vibrational frequency calculations were performed using Gaussian 09.[24] All of the molecular structures were optimized using the density functional method[25], B3LYLP hybrid density functional routine and the tight convergence criteria for optimization and the self-consistent field, SCF, was applied. Care was taken to be certain in the case of transition state that there was only one negative frequency presents in the resulting calculations. Investigations of the thermodynamic properties of the aionic and neutral structures, hindered rotation and the anharmonicity correction to the vibrational frequencies were applied. For better accuracy of the calculated values, the integrations have been performed with ultrafine grid size (Int=UltraFine). The calculated zero point energy for each method and basis set has been scaled with the proper factor before being added to the total ground-state electronic energy. A transitions state search has been done using both Berny algorithm and QST3 approach using the STQN (Synchronous Transit-Guided Quasi-Newton) method developed by Schlegel et al[26] which were found to yield almost identical results. Photodetachment spectroscopy has been used to obtain the experimental values for these quantities. Ab initio calculations using high accuracy methods such as second-order Møller-Plesset perturbation (MP2) theory or coupled clusters methods like CCSD(T) along with extended basis set can predict quantities such as VDE and VAE very accurately. The bond dissociation energy has been obtained from calculations using the following relation:[27]

$$\Delta \boldsymbol{H}^{\boldsymbol{o}}_{\boldsymbol{f},\boldsymbol{298}}(\boldsymbol{M}) = \boldsymbol{E}(\boldsymbol{M}) + \boldsymbol{ZPE}(\boldsymbol{M}) + [\boldsymbol{H}_{\boldsymbol{298}}(\boldsymbol{M}) - \boldsymbol{H}_{\boldsymbol{0}}(\boldsymbol{M})] \qquad (5)$$

$$- \sum_{\boldsymbol{z}}^{\boldsymbol{atoms}} \{\boldsymbol{E}(\boldsymbol{X}_{\boldsymbol{z}}) + [\boldsymbol{H}_{\boldsymbol{298}}(\boldsymbol{X}_{\boldsymbol{z}}) - \boldsymbol{H}_{\boldsymbol{0}}(\boldsymbol{X}_{\boldsymbol{z}})]\} + \sum_{\boldsymbol{z}}^{\boldsymbol{atoms}} \Delta \boldsymbol{H}^{\boldsymbol{o}}_{\boldsymbol{298}}(\boldsymbol{X}_{\boldsymbol{z}})$$

Since the anion under study is rather large, a number of density functional theory methods were employed to calculate the required quantities for the above relation (except for one CBS-QB3 theory calculation). To obtain the zero point energy we performed vibrational frequency calculation and the scaling factor for each level of theory and basis set has been acquired from standard references data source[28] and been applied to the results. For cases in which we could not find the exact value for scaling factor for a particular method/basis set, we applied the closest available scaling factor.

4.3 Results and Discussions

A. Electron affinity measurement experiment

The resulted photoelectron spectrum taken with 355nm laser is shown in Figure 3. One can observe that the first EBE band starts from 1.3 ± 0.1 eV and peaks at 1.78 eV. If there is sufficient Franck-Condon overlap between the ground state of the anion and the ground state of the neutral and there is not much hot band signal, the threshold of the first EBE peak, 1.3 eV, should be the electron affinity (EA). The experimental vertical detachment energy (VDE), corresponding to the peak position, is 1.78 eV.

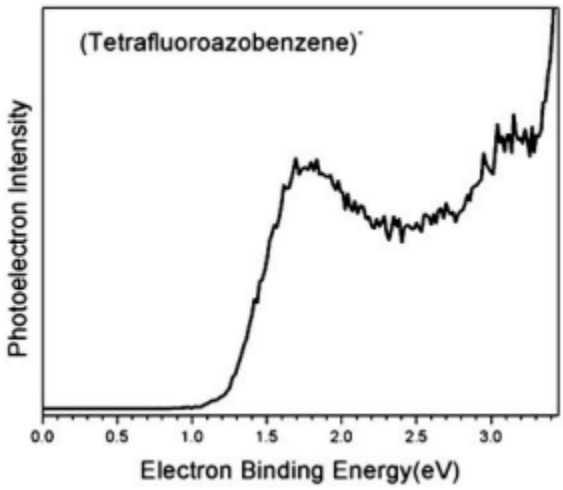

Figure. 4.3. The photoelectron spectrum of the trans-2,2',6,6'-tetrafluoro-azobenzene anion recorded using 355 nm laser line.

B. Collision induced dissociation experiment:

Figure 4 demonstrates the experimental mass spectroscopy results for 6 and 25 eV translational kinetic energy in the laboratory frame. In low energy region the predominant ion is 113 m/z peak but at higher energy the 93 and 73 m/z ions appear and their intensities grow upon increasing the collision energy. The suggested mechanism to form the three negative product ions detected in the mass spectrum can be summarized as:

$$[\boldsymbol{C_{12}H_6F_4N_2}]^- + \boldsymbol{Ar} \rightarrow \ [\boldsymbol{C_6H_3F_2}]^- + \ \boldsymbol{C_6H_3F_2N_2} + \boldsymbol{Ar} \quad (6)$$

$$[C_6H_3F_2]^- + Ar \rightarrow \ [C_6H_2F]^- + HF + Ar \quad (7)$$

$$[C_6H_2F]^- + Ar \rightarrow \ [C_6H]^- + HF + Ar \quad (8)$$

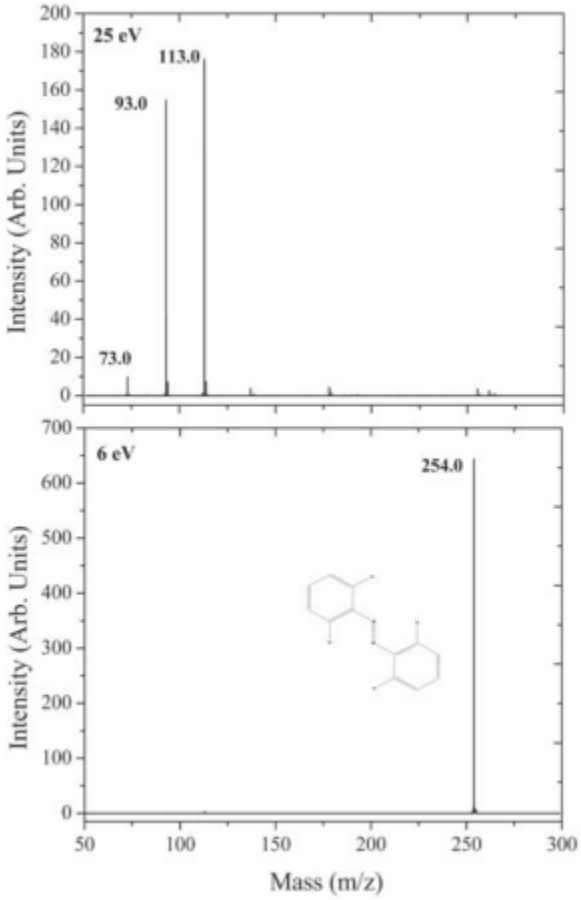

Figure. 4.4. Collision induced dissociation mass spectroscopy results for 6 and 25 eV collision energies in the laboratory frame. The 254 m/z anion is isolated with the first quadrupole and the secondary anion masses 113, 93 and 73 m/z are detected.

The energy dependence of the ion peak intensities were initially analyzed using Analyst software and then converted into a relative cross section. Deconvolution of the energy resolved collision induced dissociation cross sections was performed using the L-CID program to fit the data points and find the threshold energy. Our quantum chemistry calculations showed the energy that it takes to produce the 93 m/z anion $[C_6H_2F]^-$ directly from the parent ion through a single collision is ~4.3 eV depending upon the method and the basis set. The fact that this anion exists and shows up in the spectrum around 2.1 eV (center of mass energy) of energy which is

available for the reaction to take place proves that it cannot be the result of a single collision interaction. Since the energy resolved collision induced dissociation theory works based on the fundamental assumption that the parent ion undergoes a single collision only and the L-CID and other available codes to deconvolute the energy resolved cross section data work based on this central assumption, we will not use L-CID for deconvlution and thermochemical analysis related to 93m/z $[C_6H_2F]^-$as well as the 73m/z peak $[C_6H]^-$. The reason that they can be detected in the mass spectroscopy result can be discussed considering multiple collision theory and considering the probability of product ion collision with Argon gas (sequential dissociation). This is possible since the fragment ion has enough translational energy to overcome the dissociation barrier to produce 93 m/z peak ion. Computations using B3LYP and 6-311++G(d,p) show that this reaction will take ~2.5 eV energy. Creating the 73 m/z ion from the 93 m/z product ion in a sequential dissociation would be easier and requires only 0.65 eV kinetic energy to take place. This has been calculated using B3LYP level of theory with 6-311++G(d,p) basis set. This can explain the resemblance of the cross section data for the 93 m/z and 73 m/z peaks. Thus we will only focus on the 113 m/z peak in order to obtain the bond dissociation enthalpy for breaking the C-N bond yielding the $[C_6H_3F_2]^-$ anion and assumed $[C_6H_3F_2N_2]$ fragment. The experimental threshold dissociation energy, E_0, for for $[C_6H_3F_2]^-$ is 1.88 eV with an effective frequency of 982.4 cm^{-1} and 6.16×10^3 cm^{-1} for the α' parameter of the L-CID program. α' is the structure related parameter with the dimension of energy (cm^{-1}) which is being set by the program and is different for loose and tight transitions. Here it is assumed that the frequencies would not change much going from the starting anion to the transition state for large anions which is fair to assume for this anion. Quantum chemistry computations and mass spectroscopy results have proved that our transition type is simply a bond cleavage with no activation barrier and the transition state

qualifies as loose. Figure 5 shows the cross section data for the 113 m/z anion $[C_6H_3F_2]^-$ as a function of center of mass energy and the fit generated by the L-CID program. The bond dissociation energy resulted from this fitting, 1.88 eV, is in close agreement with the computational result of 1.93 eV (CBS-QB3 method) as will be explained in details in computational results section.

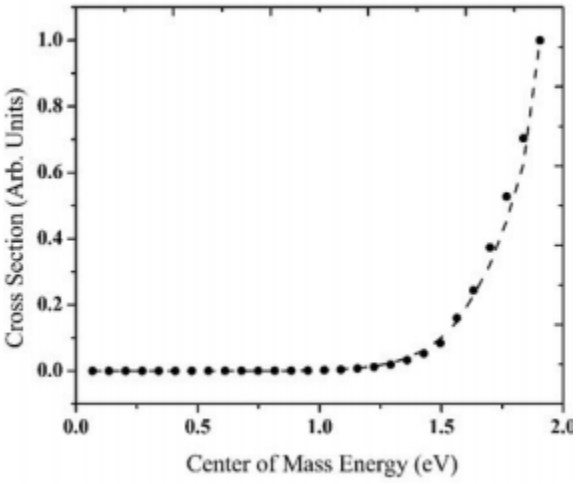

Figure.4.5 Experimental cross section (open circles) for the $[C_6H_3F_2]^-$ *product ion as a function of the energy in center of mass frame. The dashed line is the fit generated by the L-CID program.*

Figure 6 presents the experimental cross sections for 93 and 73 m/z peaks. The threshold energy for generating these two ions are close (~ 0.65 eV in center of mass frame). Computational results which will be discussed in next section provide more insight into formation of these two anions and calculated bond dissociation energies will be presented.

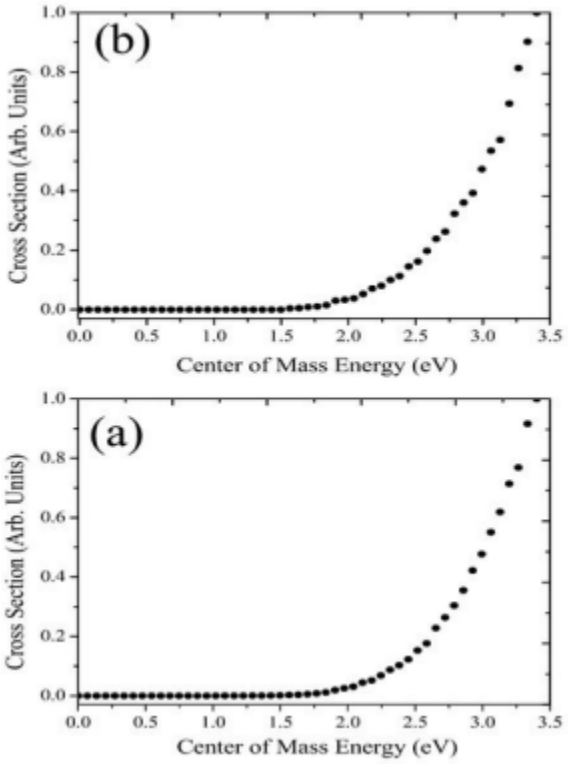

Figure. 4.6. Experimental cross sections for collision-induced dissociation as a function of kinetic energy in the center of mass frame. These ions are the result of sequential dissociation of HF from $[C_6H_3F_2]^-$ *into (a) 93 m/z peak* $[C_6H_2F]^-$ *(b) 73 m/z peak* $[C_6H]^-$.

As we discussed before since the presence of $[C_6H_2F]^-$ and $[C_6H]^-$ ions are not believed to result from single collision reactions, we are not analyzing the experimental cross section data related to those anions. Instead we present the bond dissociation energies for the reactions suggested to be reasonable for their production which are the calculated values using high level calculations. The 73 m/z peak, $[C_6H]^-$, which showed up in the spectrum at laboratory energies more than 25 eV is an especially interesting anion especially since it and other C_nH^- anions represents the first negative ion observed in the interstellar medium. McCarthy et al.[29] described the detection of $[C_6H]^-$ in the radio band in the laboratory and has been identified in the molecular envelope of IRC +10216 and in the dense molecular cloud TMC-1. Three possible

formation mechanism for this anion have been proposed previously and that includes (1) radiative attachment to $[C_6H]$, (2) charge transfer to $[C_6H]$, and (3) dissociative electron attachment to HC6X.[30]

C. Quantum Chemical Computations

The Gaussian 09 quantum chemistry code has been used for the ab initio calculations including optimizations, thermochemistry and electron affinity analysis. Calculations using B3LYP level of theory along with 6-311++G(d,p) basis set showed 2,2',6,6'-tetrafluoro-azobenzene can exist in the cis- and trans-form which are 0.36 eV different in the ground state energy which means thermodynamically the trans form is more stable. We experimentally verified that by radiating the sample in acetonitrile for about half an hour using a high power green LED and the NMR results showed the radiated sample is mostly (more than 90%) in the cis- form using NMR analysis. Table I summarizes the calculated bond dissociation energy for the trans-2,2',6,6'-tetrafluoro-azobenzene anion at 298 K. The total electronic energy and the thermochemistry data have been obtained from optimization calculation followed by a frequency calculation and care has been taken to have no any imaginary frequency in the output results. The SCF (self-consistent field) process has been performed with tight convergence criteria and the thermal correction to the enthalpy at 298 K plus the scaled zero point energy has been added to the total electronic energy. CBS methodology performs better than density functional methods in calculating bond dissociation energies with higher computational cost.

Table 4.1. Theoretical Bond Dissociation Energies (BDE) summary for cleaving the C-N bond which yields the 113 m/z ion, calculated for 298 K using different methods and basis sets.

Method/Basis set	Bond Dissociation Energy (eV)
B3LYP/6-31+G(d)	1.75
B3LYP/6-311+G(d)	1.69
B3LYP/6-311++G(d)	1.70
B3LYP/6-311++G(d,p)	1.70
B3LYP/6-311++G(2d,2p)	1.70
B3LYP/6-311++G(3df,3pd)	1.73
B3LYP/aug-cc-pVDZ	1.76
B3LYP/Lanl2DZ	2.04
M06/6-311++G(d,p)	1.97
M06-L/6-311++G(d,p)	1.99
M06-2X/6-311++G(d,p)	1.92
B3P86/6-311++G(d,p)	1.99
B3PW91/6-311++G(d,p)	1.88
wB97/6-311++G(d,p)	1.84
wB97X/6-311++G(d,p)	1.80
wB97XD/6-311++G(d,p)	1.88
CBS-QB3	1.93

Experiment	1.88 ± 0.2

We can infer from these computational results that CBS-QB3 method outcome is in excellent agreement with the experimental result, however given the estimated experimental uncertainty most of the calculations are compatible with experiment. Notice that the M06-2X global hybrid density functional theory method performs reasonably well in calculating BDE even though a large basis set was not employed. These results suggest M06-2X method is more accurate than B3LYP for thermochemical analysis. This is interesting since M06-2X does not require as much computational time as other more accurate methods such as GX or W1BD. Also wB97XD seems to perform well in calculating the bond dissociation energy in this case. Also it is clear to see that the density functional method like B3LYP results are not very sensitive to the basis set size. Table II presents the computational results for the vertical detachment energy, adiabatic electron affinity and the vertical electron affinity for the trans-2,2',6,6'-tetrafluoro-azobenzene anion. B3LYP method along with the 6-311++G(d,p) Pople basis set yields 1.67 eV for the adiabatic and 1.28 eV for the vertical electron affinity which is in reasonable agreement with experiment. The method to calculate the adiabatic and vertical molecular electron affinities and also the vertical detachment energy is explained before. In all of the calculations we optimized the geometry with tight criteria and vibrational frequency analysis has been done to find the ZPE except for the MP2 calculation in which we used the B3LYP/6-311++G(2d,2p) optimized geometry and performed the single point energy analysis on that.

Table 4.2. Summary of adiabatic electron affinity, vertical detachment energy, vertical electron affinity and the dipole moment for the neutral molecule and also the parent ion.

Method/Basis set	VDE	AEA	VEA	Neutral Dipole moment	Anion Dipole moment
B3LYP/6-31+G(d)	1.75	1.61	1.25	0.27	0.30
B3LYP/6-311+G(d)	1.80	1.65	1.27	0.29	0.34
B3LYP/6-311++G(d)	1.80	1.66	1.27	0.26	0
B3LYP/6-311++G(d,p)	1.82	1.67	1.28	0.29	0.35
B3LYP/6-311++G(2d,2p)	1.77	1.63	1.24	0.27	0
B3LYP/6-311++G(3df,3pd)	1.76	1.62	1.24	0.26	0
B3LYP/LanL2DZ	1.88	1.73	1.38	0.33	0.49
B3LYP/aug-cc-pVDZ	1.79	1.65	1.29	0.24	0
M06/6-311++G(d,p)	1.84	1.66	1.27	0.25	0.38
M06L/6-311++G(d,p)	1.68	1.56	1.24	0.34	0.45
M062X/6-311++G(d,p)	1.80	1.57	1.10	0.20	0
wB97/6-311++G(d,p)	1.81	1.50	0.91	0.20	0
wB97X/6-311++G(d,p)	1.78	1.50	0.95	0.22	0
wB97XD/6-311++G(d,p)	1.74	1.50	1.00	0.26	0
B3PW91/6-311++G(d,p)	1.80	1.66	1.28	0.30	0.34

B3P86/6-311++G(d,p)	2.36	2.21	1.85	0.29	0.29
MP2/6-311++G(d,p)	1.63	0.96	0.69	0.27	0
Experimental	1.78	1.3±0.1	-	-	-

In Table III we summarized the bond dissociation energies at 298 K based on the suggest mechanisms to create the other ions through a sequential dissociation from the primary product ion, $[C_6H_3F_2]^-$, and their dipole moments. The studied ions have been optimized with tight convergence criteria using aug-cc-pVTZ as the basis set and the ZPE was included. BDEs are in electron volt and the dipole moments are in Debye.

Table 4.3 summary of the product ions properties and the bond dissociation energies to yield (1) $[\mathbf{C_6H_2F}]^-$ and (2) $[\mathbf{C_6H}]^-$ product anions. BDEs are in electron volts unit and the dipole moments in Debye.

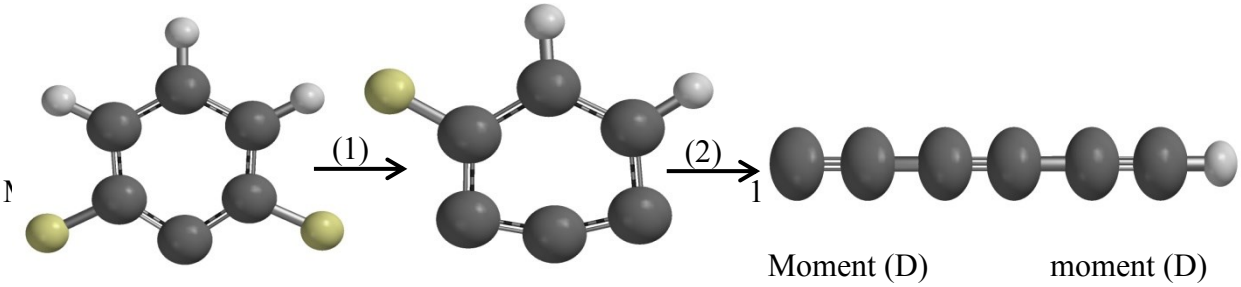

			Moment (D)	moment (D)
B3LYP	2.52	0.64	4.86	3.83
wB97XD	2.64	1.15	4.97	4.02
MP2(Full)	2.54	0.78	5.28	4.01

Calculations using B3LYP level of theory along with 6-311++G(2d,2p) basis set yields 0.99 eV, 1.94 eV and 1.47 eV for the vertical electron affinity, vertical detachment energy and the adiabatic electron affinity for the cis-form of 2,2',6,6'-tetrafluoro-azobenzene. Table IV is comparing the results for the cis- and trans-form VDE, AEA and VEA from B3LYP/6-311++G(2d,2p) level of theory computations. Notice that the neutral cis-2,2',6,6'-tetrafluoro-azobenzene has a large dipole moment which makes it possible to form a dipole bound anion as well as a valance bound anion

Table 4.4 Vertical detachment energy, adiabatic electron affinity and vertical electron affinity for cis vs trans form of 2,2',6,6'-tetrafluoro-azobenzene. Energies are in eV unit and Dipole moment is in Debye.

Conformer	VDE	AEA	VEA	Dipole
Cis	1.94	1.47	0.99	5.18
Trans	1.77	1.63	1.24	0.27

4.4 Conclusion

Ab initio calculations as well as collision induced dissociation and photoelectron spectroscopy experiments have been utilized to study 2,2',6,6'-tetrafluoro-azobenzene and its anion. Atmospheric pressure chemical ionization and thermal electron attachment was used to produce the parent $[C_{12}H_6N_2F_4]^-$ negative ion allowing collision induced dissociation and photodetachment experiments respectively. Ab initio calculations using density functional theory

yield ~1.6 eV for the adiabatic electron affinity and ~1.8 eV for the vertical detachment energy. Photoelectron spectroscopy results for the measured AEA is 1.3 ± 0.1 eV and VDE value is 1.78 ± 0.1 eV for the spectra taken with 355 nm laser wavelengths. The measured adiabatic electron affinity 1.3-1.4 eV is in reasonable agreement with our calculated value of ~1.6 eV. Collision induced dissociation of the parent anion $[C_{12}H_6N_2F_4]^-$ yields the fragment ion $[C_6H_3F_2]^-$, breakage of a CN bond. The calculated value for the bond dissociation energy for the CN bond cleavage using CBS-QB3 is 1.93 eV at 298 K which is in agreement with an experimental dissociation energy of 1.88 ± 0.2 eV from collision induced dissociation threshold measurement. The existence of $[C_6H]^-$ in our mass spectrum is attributed to subsequent losses of HF from the primary dissociation fragment, $[C_6H_3F_2]^-$. This interesting anion was the first negative ion to be detected in the interstellar medium.

Acknowledgments

We are grateful to Dr. John E. Bartmess for his kind technical help and useful discussions. We are also indebted to Dr. Andreas Bach for providing us with the L-CID program. The PD-PES experiment was supported by NSF grant, CHE-1360692.

References

[1]E. Mitscherlich, Ann. Pharm. 9, 1 (1834).

[2]T. A. Singleton, K. S. Ramsay, M. M. Barsan, I. S. Butler and C. J. Barrett, J. Phys. Chem. B, 116, 32 (2012).

[3]J. Garcia-Amoros and D. Velasco, Beilstein. J. Org. Chem. 8, 1003 (2012).

[4]G. Hartley, Nature 140, 281 (1937).

[5]S. Samanta, T. M. McCormick, S. K. Schmidt, D. S. Seferos and G. A. Woolley, Chem. Commun. 49, 87 (2013).

[6]R. Siewertsen, H. Neumann, B. Buchheim-Stehn, R. Herges, C. Nather, F. Renth and F. Temps, J. Am. Chem. Soc. 131, 43 (2009).

[7]A. Emoto, E. Uchida and T. Fukuda, Polymers. 4, 1 (2012).

[8]S. Sawada, N. Kato and K. Kaihatsu, Curr. Pharm. Biotechno. 13, 14 (2012).

[9]A. Goulet-Hanssens and C. J. Barrett, J. Polym. Sci. Pol. Chem. 51, 14 (2013).

[10]Z. Mahimwalla, K. G. Yager, J. Mamiya, A. Shishido, A. Priimagi and C. J. Barrett, Poly. Bull. 69, 8 (2012).

[11]L. Rocha, C.-M. Păiuş, A. Luca-Raicu, E. Resmerita, A. Rusu, I.-A. Moleavin, M. Hamel, N. Branza-Nichita and N. Hurduc, J. Photoch. Photobio. A: Chemistry 291, 16 (2014).

[12]S. K. Yesodha, C. K. S. Pillai and N. Tsutsumi, Prog. Polym. Sci. 29, 1 (2004).

[13]O. S. Bushuyev, A. Tomberg, T. Friščić and C. J. Barrett, J. Am. Chem. Soc. 135, 34 (2013).

[14] S.Gan, A. Yuvaraj, M. Lutfor, M. Mashitah, H. Gurumurthy, RSC Advances, 5, 9 (2015).

[15]X. Zhang, Y. Wang, H. Wang, A. Lim, G. Gantefoer, K. H. Bowen, J. U. Reveles and S. N. Khanna, J. Am. Chem. Soc. 135, 12 (2013).

[16]J. Ho, K. M. Ervin and W. Lineberger, J. Chem. Phys. 93, 10 (1990).

[17]M. Rodgers, K. M. Ervin and P. Armentrout, J. Chem. Phys. 106, 11 (1997).

[18]F. Muntean and P. Armentrout, J. Chem. Phys. 115, 3 (2001).

[19]B. H. Smith, A. Buonaugurio, J. Chen, E. Collins, K. H. Bowen, R. N. Compton and T. Sommerfeld, J. Chem. Phys. 138, 23 (2013).

[20]P. Armentrout, J. Am. Soc. Mass. Spectr. 13, 5 (2002).

[21]P. Armentrout, J. Anal. Atom. Spectrom. 19, 5 (2004).

[22]S. Narancic, A. Bach and P. Chen, J. Phys. Chem.A. 111, 30 (2007).

[23]S. E. Wheeler, A. Moran, S. N. Pieniazek and K. Houk, J. Phys. Chem.A. 113, 38 (2009).

[24]M. Frisch, G. Trucks, H. Schlegel, G. Scuseria, M. Robb, J. Cheeseman, G. Scalmani, V. Barone, B. Mennucci and G. Petersson, Gaussian, Inc. Wallingford, CT, 2009.

[25]R. Janoschek, Pure and Applied Chemistry, 73, 9(2001)

[26]C. Peng and H. Bernhard Schlegel, Isr. J. Chem. 33, 4 (1993).

[27]C. J. Cramer, Wiley, England (2004).

[28]I. M. Alecu, J. Zheng, Y. Zhao and D. G. Truhlar, J. Chem. Theory. Comput. 6, 9 (2010).

[29]M. McCarthy, C. Gottlieb, H. Gupta and P. Thaddeus, Astrophys. J. Lett. 652, 2 (2006).

[30]Y. Kasai, E. Kagi and K. Kawaguchi, Astrophys. J. Lett. 661, 1(2007).

Chapter 5. Electron-Induced Proton Transfer in 2-Hydroxypyridine Dimer: An Anion Photoelectron Spectroscopic and Density Functional Theory Study

Yi Wang[1], Sarah T. Stokes[2], Xinxing Zhang[1], Alexandra Vlk[2], and Kit H. Bowen Jr.[1]

[1]Department of Chemistry, Johns Hopkins University, Baltimore, MD 21218, USA

[2]Department of Chemistry, Towson University, Towson, MD 21204, USA

Abstract

Anion photoelectron spectroscopic and theoretical studies on the dimer anion of (2-hydroxypyridine)$_2^-$ are reported. The experimentally measured vertical detachment energy (VDE) is 1.21eV, which compares well with the theoretically predicted values using density functional theory calculations. Experimental and theoretical findings confirm that the proposed intermolecular electron induced proton transfer process occurs in the dimer anion.

5.1 Introduction

Electron-induced proton transfer occurs in many biologically related reactions. When low-energy electrons are produced by ionization as a result of high-energy radiation, the excess electron is likely to attach onto a DNA base pair leading to barrier-free proton transfer. Such a process has been suggested as the key step in DNA tautomerization and considered to be the cause of damage to DNA molecules in cells[1-4].

In 2012, Gerardi et al. conducted photoelectron spectroscopic study on formic acid dimer anions, aiming to investigate the mechanism of DNA damage by electron induced proton transfer. They found electron attachment induced the proton transfers in the cyclic, multiple H-bonding motif found in DNA base pairs. Theoretical and spectroscopic studies show that the proton transfer process results in the formation of a formate anion and a dihydroxymethyl radical linked by two hydrogen bonds. The single occupied molecular orbital shows that the excess electron is delocalized in the conjugated π orbitals on dihydroxymethyl radical.

The 2-hydroxypyridine dimer had been studied both experimentally and theoretically, due to its structural similarity to DNA base pairs. More than a decade ago, Borst et al. conducted an ultraviolet and infrared spectroscopic study on hydrogen bonding in the 2-hydroxypyridine dimer and proposed an excited state double proton transfer tautomerization. They found that double proton tunnelling occurs only in excited states (S_1-S_0) [9]. However, no evidence shows proton transfer as neutral ground state experimentally.

Other spectroscopic studies performed on the neutral and cationic forms of 2-hydroxypyridine include ultra-violet and infrared [9], NMR[10], microwave[11], Zero Electron Kinetic Energy (ZEKE)[12] and time-resolved spectroscopy[13]. The geometries, vibrational and rotational features were extensively studied using density functional theory[14-17] and

Moller-Plesset perturbation theory. Both experimental and theoretical work on the negatively charged 2-hydroxypyridine are scarce.

Here we present the negative ion photoelectron spectroscopic study of the 2-hydroypyridine dimer. The vertical detachment energy of the 2-hydroypyridine dimer anion obtained from the photoelectron spectrum is 1.21eV. Geometry and energy calculations on different 2-hydroxypyridine tautomers were studied utilizing density functional theory, which supported our experimental results very well. The theoretical calculations also supported our proposed electron induced proton transfer process, and indeed, no proton transfer occurred as the neutral dimer which agrees with literature results[9].

5.2 Experimental Methods

Negative ion photoelectron spectroscopy is conducted by crossing a mass-selected beam of negative ions with a fixed-frequency beam of photons and energy-analyzing the resultant photodetached electrons. This technique is based on the energy conserving relationship, $h\nu$ = EKE + EBE, where EKE is electron kinetic energy, EBE is electron binding energy, and $h\nu$ is the photon energy. In the present experiment, negative ions were formed in a supersonic expansion nozzle-ion source. There, the 2-hydroxypyridine was placed in a stagnation chamber, heated to 40-50 ^{o}C, and co-expanded with 2-3 atm of argon gas through a 23 μm orifice into a 10^{-4} torr vaccum. A hot, negatively biased thoriated iridium filament injected low energy electrons, in the presence of a weak magnetic field, into the resulting gas expansion, producing negative ions. These anions were then extracted, collimated, and transferred into the flight tube of a 90◦

magnetic sector mass spectrometer with a typical mass resolution of 400. The mass-selected anions of interest were then crossed with the intracavity laser beam of an argon ion laser, operating at 2.54 eV/photon (488 nm), and the resulting photodetached electrons then energy analyzed in a hemispherical electron energy analyzer with a typical resolution of 25 meV. Photoelectron spectra of the 2-hydroxypyridine anions were calibrated against the well-known spectrum of O^-. A detailed description of our apparatus has been given elsewhere [19].

Computational Methods

Density functional theory (DFT) calculations of the 2-hydroxypyridine neutral and anion were performed by applying the wb97xd[20] functional using the Gaussian09 software package [21]. The geometries of anions and their corresponding neutrals were fully optimized using the 6-31+G (p,d) basis set [22-23]. The electronic energies were then improved by single–point calculations using the 6-311++*G*(3d,3pd) basis set at optimized geometries[24]. The highest occupied molecular orbital (HOMO) of the relaxed anion was generated in GaussView.

5.3 Results and Discussion

The photoelectron spectrum of the 2-hydroxypyridine dimer is shown in Figure.1. The intensity maximum in the photoelectron spectrum gives the experimental VDE, which is 1.21eV. In comparison with dipole bond anion PES, which features a narrow sharp peak at low electron binding energy, typically under 0.5eV[25], the relatively large VDE indicates that under these experimental conditions, a stable valence dimer anion is produced. Our previous studies on DNA bases indicate that the large VDE, usually over 1eV, along with the broad band in the PES,

are the result of an electron-induced proton transfer process. The excess electron resides in the π* orbital of the neutral proton transferred radical[2-4, 25-27]. The resultant radical interacts with its deprotonated counterpart. The experimental PES, along with the theoretical results show that proton transfer occurs within the 2-hydroxypyridine dimer.

Since 2-hydroxypyridine exists in two tautomeric forms, we carried out DFT calculations on geometries of three possible tautomers of the 2-hydroxypyridine dimer, both anions and neutrals (see Figure.2). The calculated absolute energies, bond lengths, and VDEs are tabulated in Table.1. The geometry optimizations of all three dimer neutrals indicate that none of them undergo the proton transfer process. However, all three dimer anions clearly undergo the proton transfer process, resulting in a newly formed O-H bond. Calculated bond lengths of the newly formed O-H bond in each anion are 1.174 Å and 1.178 Å, comparable with a typical O-H bond length of 0.96Å, which suggests that the proton is successfully transferred. It is worth noticing that after the proton is transferred, resultant anions, $(2\text{-hydroxypyridine})_2^-$ and $(2\text{-pyridone})_2^-$ have the exact same structure (1a in Figure.2). A possible double proton transfer pathway can be implied due to the fact that the electron attachment on $(2\text{-hydroxypyridine})_2$ and $(2\text{-pyridone})_2$ result in the same anion structure. The hypothetical process can be: 1. the electron attaches onto either $(2\text{-hydroxypyridine})_2$ or $(2\text{-pyridone})_2$ to make the dimer anion; 2. the electron is detached from the anion and forms the neutral dimer. Since the two neutral tautomers have similar energy, the electron detachment may result in either one of the neutral dimers. Thus, a double proton transfer process may take place. Comparing the absolute energy of 1a and 2a, we noticed that 1a is slightly energy favored. That might be due to the repulsion between the two hydrogens on the 5 position carbons.

The 2-hydroxypyridine – 2-pyridone tautomerization given in scheme 1, favors the 2-hydroxypyridine (lactim) in the gas phase; 2-hydroxypyridine, and its tautomer 2-pyrinone, is a classic case of lactum-lactim tautomerization(See scheme). The tautomeric mechanism has long been of interest to chemists[5-7]. It exists in two tautomeric forms, 2-hydroxypyridine (lactim form), and 2-pyridone (lactam form). In the gas phase, the lactim form is slightly energy favoured while in polar solvents, the lactam form dominates[8]. If one views the polar solvent as being a second 2-hydroxypyridine molecule (now a dimer system) one expects that the 2-pyridone form of the neutral dimer, 2n should be favored over the 2-hydroxypyridine dimer form, 1n. We see very little difference in energy for these two forms and conclude that perhaps self-solvation with only one additional molecule (to make the dimer) is not enough to cause the expected solvent effect. Studies of larger homogenous clusters or other polar solvents (e.g. water) could be conducted to potentially monitor the preference of the lactam vs. lactim form as number of solvent molecules increase. The VDEs of 1a and 2a are found to be very close, 1.15eV and 1.20eV respectively. Figure.3 shows the HOMO of relaxed anions 1a, indicating the excess electron is delocalized in the $\pi*$ anti-bonding orbital of the protonated neutral parents, which is consistent with our previous findings on DNA base pairs[25-27]. This was also consistent with Johnson's finding.

5.4 Summary

The photoelectron spectrum of the 2-hydroxypyridine dimer anion was recorded utilizing a 2.540eV photon laser. The VDE was determined to be 1.21eV-which agreed excellently with both of our calculated VDEs of the two tautomers using the DFT method. The intermolecular electron induced proton transfer was confirmed by both the experimental results and the

calculated geometry. A possible double proton transfer mechanism was proposed and can be helpful to have a better understanding of DNA base pairs.

5.5 References

1. B. Boudaiffa, P. Cloutier, D. Hunting, M.A. Huels, L. Sanche, *Science* 287, 1658 (2000)
2. I. Dabkowska, J. Rak, M. Gutowski, J. M. Nilles, S. T. Stokes, D. Radisic, and K. H. Bowen Jr., *Phys. Chem. Chem. Phys.*, 6, 4351-4357 (2004).
3. I. Dabkowska, J. Rak, M. Gutowski, J. M. Nilles, S. T. Stokes, and K. H. Bowen Jr., *J. Chem. Phys*., 120, 6064-6071 (2004).
4. A. Szyperska, J. Rak, J. Leszczynski, X, Li, Y. J. Ko, H. Wang, and K. H. Bowen, *Chem. Phys. Chem*, 11, 880-888 (2010)
5. Yen, S. J., Ho J. J. *J. Phys. Chem. A.*, 104, 8551 (2000).
6. Nyguyen K. A., Gordon M. S., Truhlar D. G., *J. Am. Chem. Soc.*, 113, 1596 (1991).
7. Chou P. T., Wei C. Y. *J Phys. Chem. B*, 101, 9119 (1997).
8. D. Ray, A. Pramanik and N. Guchhait, *J. Photochem. Photobiol., A*, 274, 33 (2014).
9. D.R. Borst, J.R. Roscioli, D.W. Pratt, G.M. Florio, T.S. Zwier, A. Müuller, S. Leutwyler *Chem. Phys*., 283, 341 (2002).
10. Szyc, Ł.; Guo, J.; Yang, M.; Dreyer, J.; Tolstoy, P. M.; Nibbering, E. T. J.; Czarnik-Matusewicz, B.; Elsaesser, T.; Limbach, H.-H. *J. Phys. Chem. A*, 114, 7749 (2010).
11. Tanjaroon, C. Subramanian, R. Karunatilaka, C., and Kukolich, S. G.,*J. Phys. Chem. A* 108, 9531 (2004).
12. Ozeki H., Cockett M. C. R., Okuyama,s K., Takahashi M., and Kimura K., *J. Phys. Chem.* 1995, 99, 8608-8612
13. H. Sekiya, K. Sakota, J. Photochem. Photobiol. C-Photochem. Rev., 9 81 (2008).
14. D. Wu, L. Liu , G. Liu , and D. Jia *J. Phys. Chem. A*, 111 5244 (2007).
15. A. Dkhissi, R. Ramaekers, L. Houben, L. Adamowicz, G. Maes, Chem. Phys. Lett., 331, 553

(2000)

16. M. Meuwly, A. Müller, S. Leutwyler, *Phys. Chem. Chem. Phys*. 5, 2663–2672. (2003).
17. E. Sagvolden, F. Furche, and A. Kohn *J. Chem. Theory Comput*. 2009, 5, 873–880
18. H. Schlegel , P. Gund , and E. Fluder, J. Am. Chem. Soc., , 104 (20), pp 5347–5351 (1982).
19. Coe, J. V.; Snodgrass, J. T.; Freidhoff, C. B.; McHugh, K. M. Bowen, K. H. *J. Chem. Phys.*, 84, 618−625. (1986).
20. J.-D. Chai and M. Head-Gordon, Phys. Chem. Chem. Phys.10, 6615 (2008).
21. Gaussian 09, Revision A.2, M. J. Frisch, G. W. Trucks, H. B. Schlegel, G. E. Scuseria, M. A. Robb, J. R. Cheeseman, G. Scalmani, V. Barone, B. Mennucci, G. A. Petersson, H. Nakatsuji, M. Caricato, X. Li, H. P. Hratchian, A. F. Izmaylov, J. Bloino, G. Zheng, J. L. Sonnenberg, M. Hada, M. Ehara, K. Toyota, R. Fukuda, J. Hasegawa, M. Ishida, T. Nakajima, Y. Honda, O. Kitao, H. Nakai, T. Vreven, J. A. Montgomery, Jr., J. E. Peralta, F. Ogliaro, M. Bearpark, J. J. Heyd, E. Brothers, K. N. Kudin, V. N. Staroverov, R. Kobayashi, J. Normand, K. Raghavachari, A. Rendell, J. C. Burant, S. S. Iyengar, J. Tomasi, M. Cossi, N. Rega, J. M. Millam, M. Klene, J. E. Knox, J. B. Cross, V. Bakken, C. Adamo, J. Jaramillo, R. Gomperts, R. E. Stratmann, O. Yazyev, A. J. Austin, R. Cammi, C. Pomelli, J. W. Ochterski, R. L. Martin, K. Morokuma, V. G. Zakrzewski, G. A. Voth, P. Salvador, J. J. Dannenberg, S. Dapprich, A. D. Daniels, Ö. Farkas, J. B. Foresman, J. V. Ortiz, J. Cioslowski, and D. J. Fox.
22. J. S. Binkley, J. A. Pople, and W. J. Hehre, *J. Am. Chem. Soc.*, 102(1980) 939-47.
23. M. S. Gordon, J. S. Binkley, J. A. Pople, W. J. Pietro, and W. J. Hehre, *J. Am. Chem. Soc.*, 104 (1982) 2797-803.
24. A. D. McLean and G. S. Chandler, J. Chem. Phys., 72 (1980) 5639-48.
25. J.H. Hendricks, S.A. Lyapustina, H.L de Clercq, J.T. Snodgrass and K.H. Bowen, J. Chem.

Phys. 104, 7788 (1996).

26. D. Radisic, K.H. Bowen, I. Dabkowska, P. Storoniak, J. Rak and M. Gutowski, J. Am. Chem. Soc. 127, 6443 (2005).

27. Yeon Jae Ko, Haopeng Wang, Dunja Radisic, Sarah T. Stokes, Soren N. Eustis Kit H. Bowen, Kamil Mazurkiewicz, Piotr Storoniak, Arkadiusz Kowalczyk, Maciej Haranczyk, Maciej Gutowski, and Janusz Rakb, Molecular Physics Vol. 108, 2010, 2621–2631.

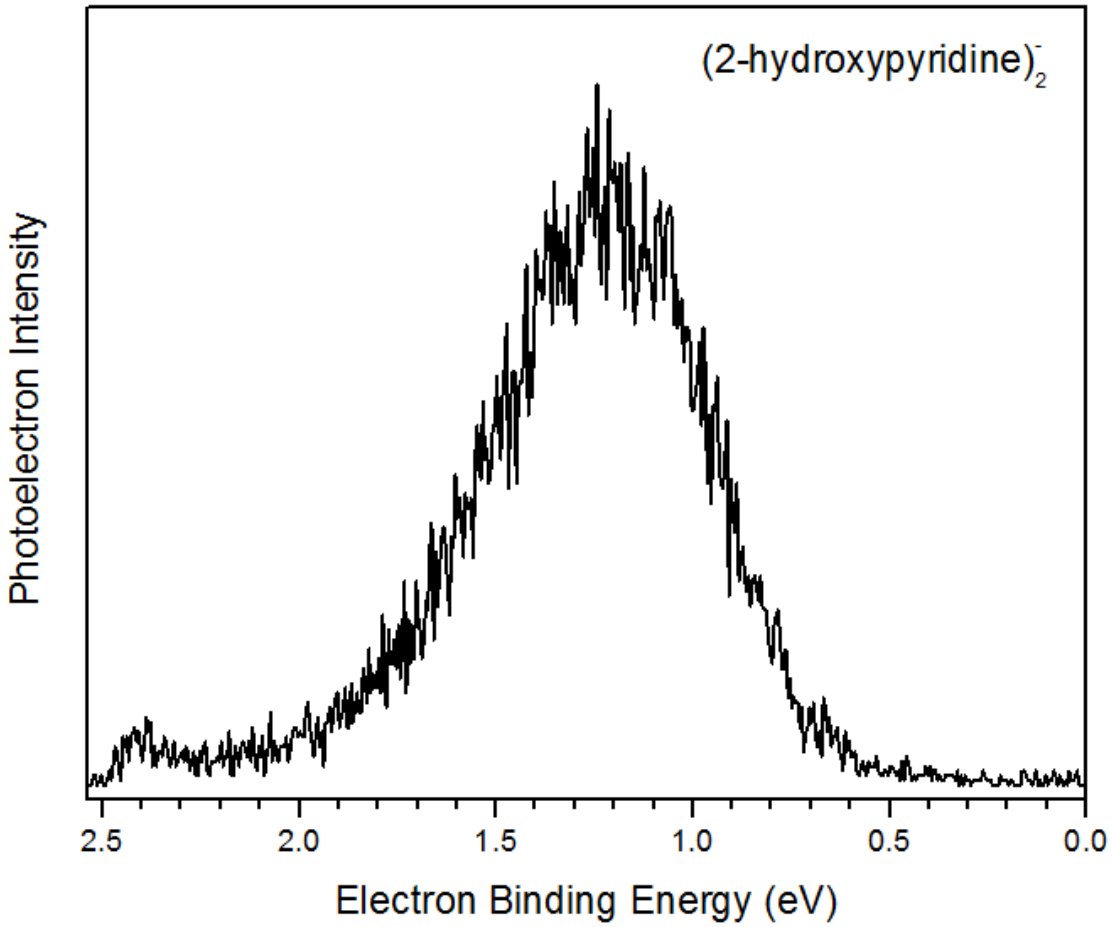

Figure 5.1: The measured photoelectron spectrum of the (2-hydroxypyridine)$_2^-$ anion recorded using 2.540 eV photons.

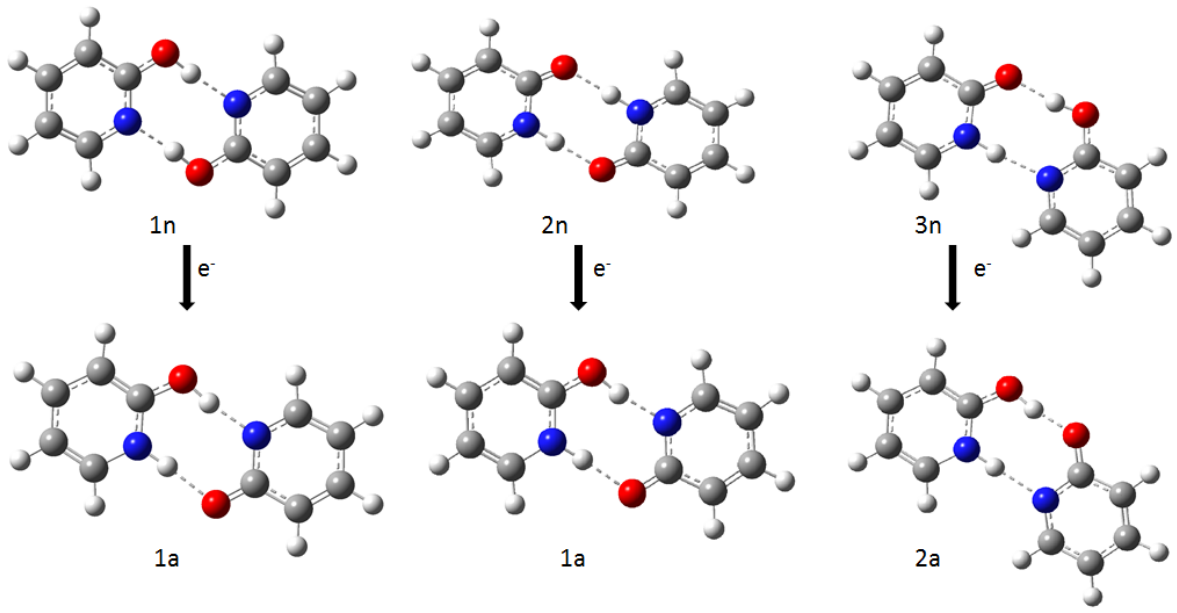

Figure 5.2: Electron-induced proton transfer in three 2-hydroxypyridine dimer tautomers: neutral 2-hydroxypyridine dimer, 2-pyridone dimer and 2-hydroxypyridine-2-pyridone dimer are noted as 1n, 2n, 3n respectively. The anions are noted as 1a and 2a accordingly.

Table.5. 1: Calculated and experimental vertical detachment energies, absolute energies and newly formed O-H bond length of (2-hydroxypyridine)$_2^-$.

	Absolute Energy(Hartree)	Calculated VDE(eV)	Experimental VDE(eV)	O-H Bond Length (Å)
1n	-647.0358918			
1a	-647.0782765	1.15	1.21	1.174
2n	-647.0358923			
1a	-647.0782765	1.15		1.174
3n	-647.0335289			
2a	-647.0777499	1.20		1.178

Scheme.1 Tautomerization of 2-hydroxypyridine/2-pyridone

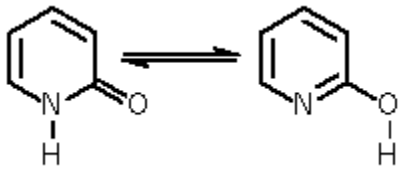

Figure 5.3: The highest occupied molecular orbital (HOMO) of the ground state of the (2-hydroxypyridine)$_2^-$ anion at the wb97xd/6-31+G (p,d) level of theory.

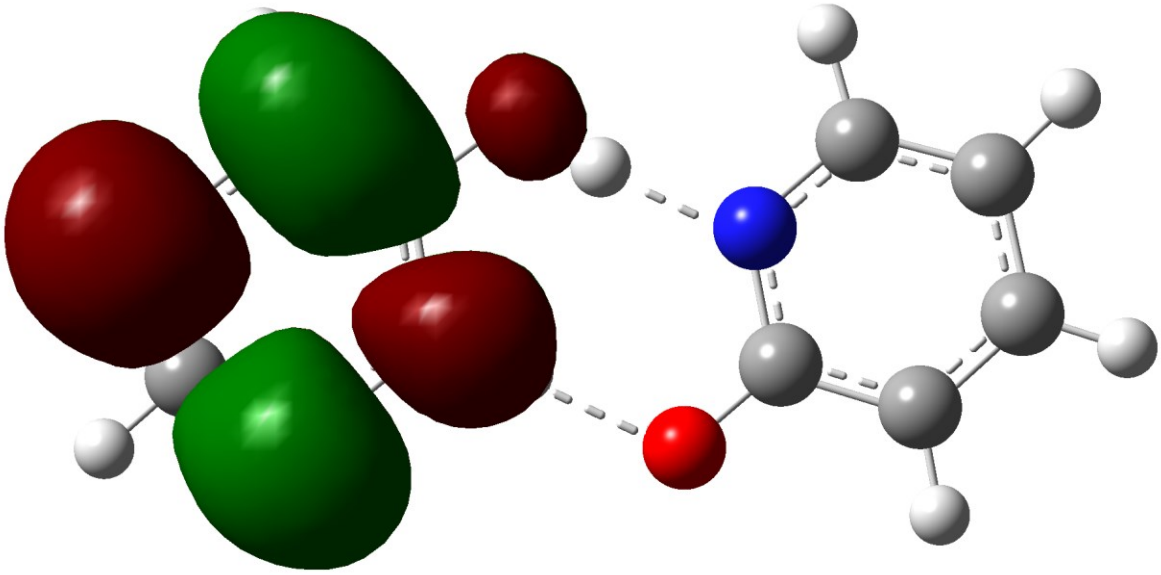

Chapter 6. Onset of Electron Induced Proton Transfer in N-Heterocyclic Azabenzenes

Yi Wang[‡], John T. Kelly[†], Xinxing Zhang[‡], Gaoxiang Liu[‡], Jacob Graham[‡], Kit H. Bowen[‡], Gregory S. Tschumper[†] & Nathan I. Hammer[†]

[†]Department of Chemistry and Biochemistry, University of Mississippi, P.O. Box 1848, University, Mississippi 38677, United States

[‡]Department of Chemistry, Johns Hopkins University, 3400 North Charles Street, Baltimore, Maryland 21218, United States

Keywords: Hydrated Anions, Photoelectron Spectroscopy, Density Functional Theory

Abstract

The transfer of a proton from water to explicitly solvated N-heterocyclic azabenzene bases is induced by the addition of an excess electron and studied here using photoelectron spectroscopy and computational chemistry. The onset of proton transfer requires a different number of solvated water molecules, depending upon the number of nitrogen atoms and their positions in the conjugated ring. In the case of s-triazine ($C_3H_3N_3$), which has a positive electron affinity, proton transfer is not energetically favored or observed experimentally. Heterocyclic rings with only 1 or 2 nitrogen atoms have negative electron affinities, but the addition of solvating water molecules can yield stable negative ions. In the case of the diazines ($C_4H_4N_2$) pyrazine, pyrimidine, and pyridazine, the addition of one water molecule stabilizes a negative ion with the majority of the excess electron density in a * orbital of the heterocycle and not significantly extended into the hydrogen bonded water network. Pyridine (C_5H_5N), with the most negative electron affinity, requires three water molecules to stabilize a negative ion. Although our computations suggest proton transfer is energetically viable when at least three water molecules are present in these clusters, it is not observed experimentally in the triazine nor diazine series. In pyridine, proton transfer competes energetically with hydrogen bonding when

three water molecules are present. Pyridine clusters containing four or more water molecules almost exclusively exhibit proton transfer and subsequent solvated hydroxide ions. Employing a previously developed hydration extrapolation technique we also determine the electron affinities of the azabenzenes pyrazine, pyridazine, and pyridine to be 0.0 eV, -0.1 eV, and -0.5 eV.

6.1 Introduction

Subtle noncovalent interactions between nitrogen containing heterocyclic molecular building blocks such as the azabenzenes, shown in Figure 1, and hydrogen bonded aqueous environments play important roles in both biological structure and function. Such interactions are essential for macromolecular assembly from the DNA double helix comprised of nucleotides to the folding of proteins.[1-7] The interactions between water and ions are involved in important biochemical processes, aqueous electrolyte chemistry and atmospheric chemistry.[8-10] Such hydrogen bonded networks have been studied at the nanoscopic level for decades to understand such interactions.[11,12] The addition of an excess electron to these systems alters the energetic landscape and here we explore how noncovalent interactions are adjusted with respect to stepwise hydration to stabilize an excess electron.

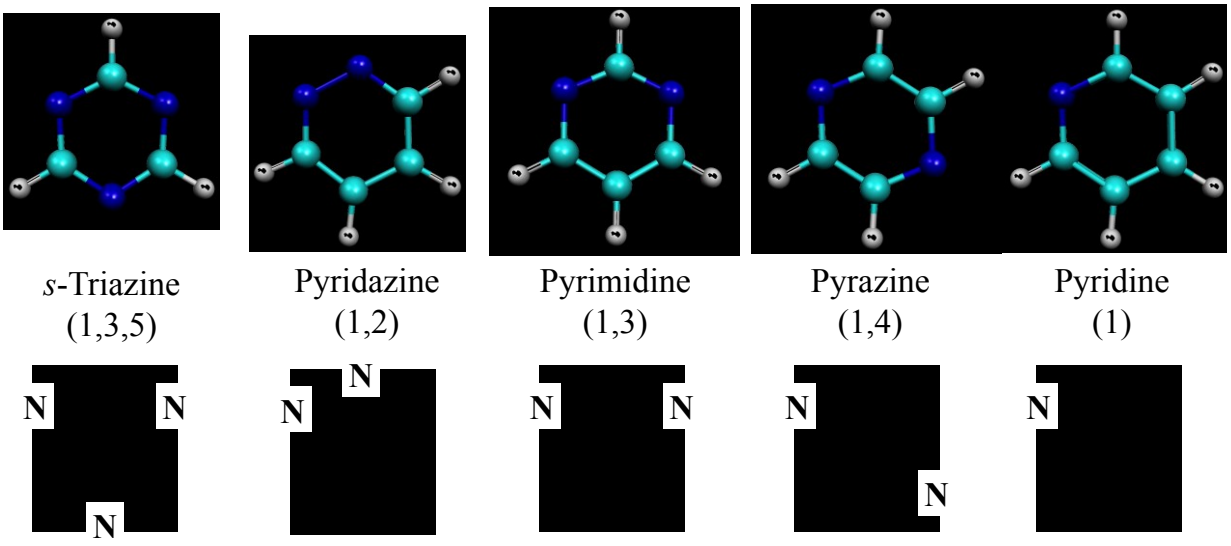

Figure 6.1: The five N-heterocyclic azabenzene anions in this study: s-triazine (Tz), pyridazine (Pd), pyrimidine (Pm), pyrazine (Pz), and pyridine (Py).

In 1975, Nenner and coworkers employed electron transmission spectroscopy and polarography to compare the electron affinity (EA) of benzene to isoelectronic azabenzenes (Figure 1). The EA of benzene (–1.15 eV) was reported to be much more negative than that of pyridine (–0.62 eV) and the EAs of the diazines were closely approaching zero.[13] Periquet et al. showed that pyridine, along with all of the diazines, have negative electron affinities but that the addition of water molecules stabilized their negative ions.[14] We recently confirmed that the pyrimidine anion was unstable with respect to autodetachment but the addition of a single water molecule stabilized the Pm negative ion.[15] Negative ion photoelectron spectroscopy has previously estimated the EA of Py to be between –0.67 eV and –0.15 eV, Pz to be –0.01 eV, and *s*-trazine to have a positive EA of +0.03 eV.[16-18] The azabenzene series has also shown interesting "associative" bond formation to CO_2 upon electron attachment.[19,20]

Here, we explore the effects of sequential hydration of the azabenzenes on the ability of these molecules' to accommodate an excess electron. In a combined photoelectron spectroscopic and computational study, we quantify the electron affinities of the azabenzenes using a previously developed hydration extrapolation[15] and explore the onset of proton transfer to create solvated hydroxide ions as a function of the number of solvated water molecules. This investigation focuses on the energetic favorability of proton transfer based the position of nitrogen atoms in hydrated azabenzene anion clusters

6.2 Experimental Details

Mass selected negative ions were crossed with a fixed energy photon beam resulting in photodetached electrons that were analyzed using a magnetic-bottle photoelectron spectrometer (resolution ~30 meV) as described previously.[21-24] This technique is governed by the well-known

relation, h =EBE+EKE, where h EBE, and EKE are the photon energy, the electron binding energy (transition energy), and the electron kinetic energy, respectively. In the supersonic expansion, individual azabenzene and water molecules were co-expanded with argon to create hydrated cluster anions.

6.3 Computational Details

A similar computational approach from our previous study has been employed using the Gaussian09 software package to perform full geometry optimizations as well as harmonic frequency calculations.[25] A hybrid meta-GGA functional, M06-2X,[26-28] was employed for the hydrated azabenzene anions to compare relative energetics as well as compute vertical detachment energy (VDE). Pure angular momentum (5*d*,7*f*) atomic orbital basis functions along with a pruned numerical integration grid composed of 99 radial shells and 590 angular points per shell was employed. All electronic structure methods utilized a Popel-style double-ζ basis set, 6-31++G(*d*,*p*). Our previously optimized neutral[29] and anionic[15] structures were taken as starting geometries for all of the hydrated azabenzene series. Additional starting geometries were generated by attaching an azabenzene molecule to a free hydrogen atom from known water cluster geometries[30-36] and hydrated electron clusters. [37-49] Though not an exhaustive conformational search, this study identifies low energy structures that should be close to the global minimum. VDEs were calculated as the difference between the optimized electronic energy of the anion and that of the corresponding neutral species with identical geometry. A previously developed solvent polarized continuum model (PCM) linear extrapolation[50] revealed that the ordering of the electron affinities are as followed: pyridine (1) > pyrimidine (1,3) > pyridazine (1,2) > pyrazine (1,4) > s-triazine (1,3,5).

6.4 Experimental Results

Figure 2 shows the photoelectron spectra (PES) of the first four solvated cluster anions for each of the azabenzene molecules studied here. Additional experimental photoelectron spectra are included in the Supporting Information. Broad spectral features are typical of such hydrated valence anions and their EAs also tend to increase with each sequential hydration, $A^{-}\cdot(H_2O)_n + H_2O \rightarrow [A\cdot(H_2O)_{n+1}]^{-}$.[51,52] We recently reported PES of the hydrated pyrimidine series for n = 1-8 and have included those results here for comparison. [15]

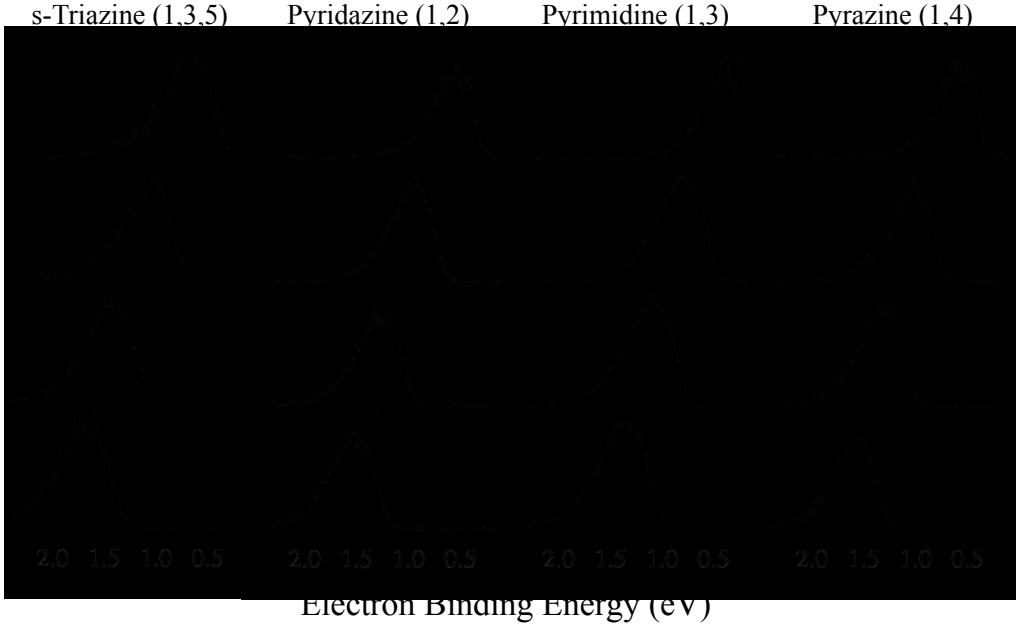

Figure 2: Photoelectron spectra of the first four stable hydrated azabenzene anion clusters: $Tz^{-}\cdot(H_2O)_n$, $Pd^{-}\cdot(H_2O)_n$, $Pm^{-}\cdot(H_2O)_n$, and $Pz^{-}\cdot(H_2O)_n$,where n = 1 – 4.

4.1 Hydrated s-Triazine Anions

S-Triazine anion, Tz^-, is the only isolated azabenzene considered here that exhibits a stable bound state with respect to autodetachment. Kim et al. previously reported the gas phase photoelectron spectrum of the Tz molecular anion and examined the effects of Jahn-Teller distortion via indirect evidence of asymmetric charge distribution. The assigned electron affinity was described to be 0.03 eV.[17] The photoelectron spectra of the hydrated Tz cluster anion series is shown in Figure 3A. The experimental VDE for $n = 1$ is 0.68 eV. The VDEs are observed to increase continuously with hydration and are 1.01 eV, 1.41 eV, 1.69 eV, 1.89 eV, and 2.09 eV, for $n = 2 – 6$, respectively.

4.2 Hydrated Pyridazine, Pyrimidine, and Pyrazine Anions

Pyridazine is the diazine derivative of pyridine with the second nitrogen atom in the *ortho-* position (i.e. 1,2 diazine). The electron affinity of the Pd molecular anion has been speculated to be slightly negative. [13] With the addition of a single water molecule and the monohydrated cluster anion is stabilized and exhibits a VDE of 0.53 eV. Addition of subsequent water molecules leads to VDEs of 0.93 eV, 1.27 eV, and 1.53 eV for n=2–4, respectively.

We previously reported PES of the hydrated pyrimidine series up to $n = 8$ and have included those results here for comparison. The VDEs of the hydrated pyrimidine anion series are 0.42 eV, 0.78 eV, 1.11 eV, 1.34 eV, 1.58 eV, and 1.62 eV, respectively, while the extrapolated electron affinity of the pyrimidine monomer was reported to be 0.2 eV.

Pz is another derivative of Py with the second nitrogen atom in the *para-* or 1,4 position of the heterocycle (see Figure 1). Kim et al. previously estimated the EA of pyrazine to be -0.01 ± 0.01 eV using a sequential argon extrapolation.[18] The photoelectron spectra of hydrated Pz

series is shown in Figure 3 and results in experimental VDEs of 0.66 eV, 1.05 eV, 1.32 eV, and 1.60 eV for *n*=1-4, respectively.

4.3 Hydrated Pyridine Anions

The experimental photoelectron spectra of hydrated pyridine cluster anions are shown in Figure 3. The $[A\cdot(H_2O)_n]^-$, n = 1,2, clusters are unstable in the gas phase with respect to autodetachment. The PES for *n*=3 exhibits two broad overlapping features with a smaller peak centered at 0.88 eV and a larger feature centered at 1.56 eV. PES for *n*=4-6 each exhibit a single broad feature with experimental VDEs of 1.79 eV, 1.98 eV, and 2.18 eV, respectively.

Figure 6.3: Photoelectron spectra of the first four stable hydrated azabenzene anion clusters: $[Py\cdot(H_2O)_n]^-$,where n = 3 – 6.

6.5 Theoretical Results

Over 80 hydrated cluster anion structures for the selected azabenzene series that corresponds to minima (no imaginary frequencies) were characterized and are included in the Supporting Information. The low-energy structures identified in this calibrated DFT procedure[53] exhibits two solvation motifs. The identified lowest energy structures for the di- and triazine heterocycles display a motif in which an extended hydrogen bonded network is formed where water molecules interact with a single nitrogen atom of the azabenzene for anion clusters where $n \geq 2$. These structures are characterized by the majority of the excess electron density residing in a * orbital and not significantly interacting with the extended hydrogen bonded water network. Clusters exhibiting this structural motif are indicated by $A^{-}\cdot(H_2O)_n$ (A = Tz, Pd, Pm, Pz, Py) and are the lowest energy structures for Tz, Pz, Pm, and Pd, which are shown in Figure 4.

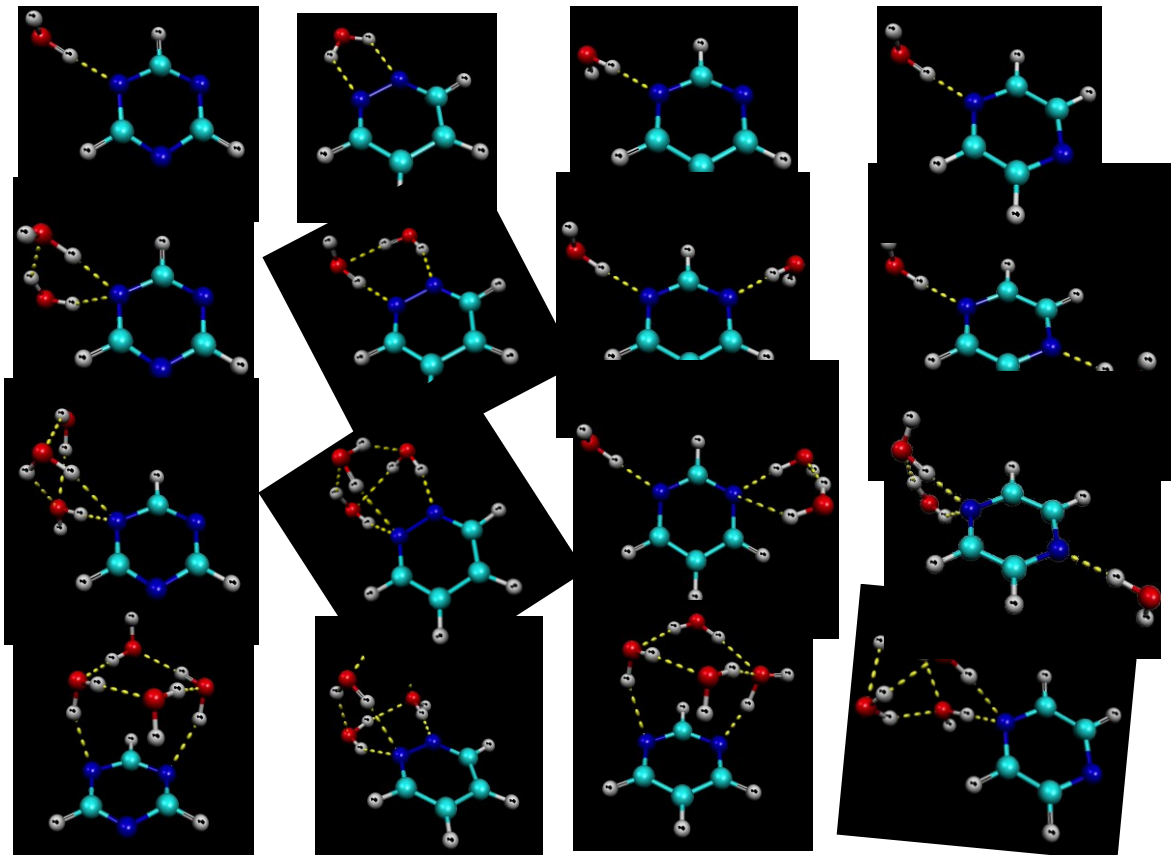

Figure 6.4: Lowest energy structures (from top to bottom) for $Tz^{-}\cdot(H_2O)_n$, $Pd^{-}\cdot(H_2O)_n$, $Pm^{-}\cdot(H_2O)_n$, and $Pz^{-}\cdot(H_2O)_n$ for n=1-4.

Starting with n = 3 in Py and Pd (n = 4 in Pm, Pz, and Tz), another type of low-energy structure emerges in where a proton from a water molecule transfers to the azabenzene effective creating an ion complex $[AH\cdot OH]^{-}$. This structural motif is denoted by $[AH\cdot OH]^{-}\cdot(H_2O)_{n-1}$. In the case of Py, the lowest energy structures for each cluster size for $n \geq 3$ exhibit proton transfer. These are shown in Figure 5 with $Py^{-}\cdot(H_2O)_3$ included for comparison. In the other azabenzenes, however, structures exhibiting proton transfer are never the lowest energy structures.

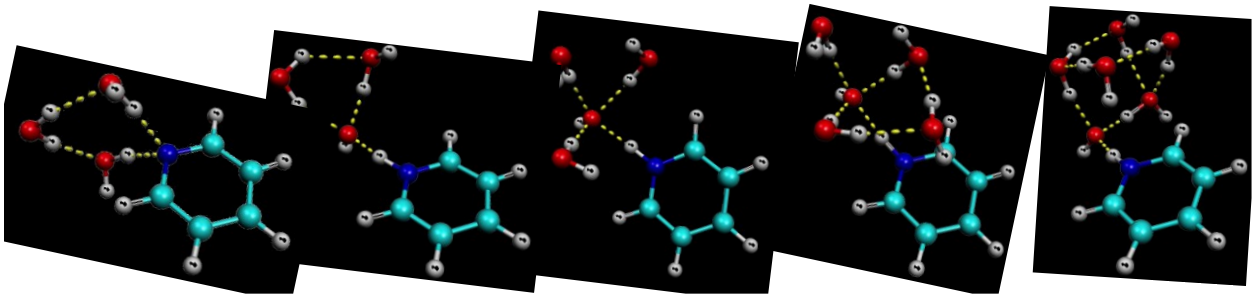

Figure 6.5: From left to right: Low-energy structures for $Py^{-}\cdot(H_2O)_3$, $[PyH\cdot OH]^{-}\cdot(H_2O)_2$, $[PyH\cdot OH]^{-}\cdot(H_2O)_3$, $[PyH\cdot OH]^{-}\cdot(H_2O)_4$, and $[PyH\cdot OH]^{-}\cdot(H_2O)_5$.

5.1 Hydrated s-Triazine Anions

The heterocycle *s*-triazine is the only isolated azabenzene anion in this study that has a positive electron affinity and is stable with respect to autodetachment. The addition of an excess

electron lowers the symmetry of *s*-triazine from D_{3h} to C_{2v} due to Jahn-Teller distortions. Since the anion and neutral species are nearly isoenergetic, the addition of a single water molecule can further stabilize the excess electron for structural assessment as well as understand binding motifs and charge localization in hydrated azabenzene anions. The $Tz^{-}\cdot(H_2O)_{n=1\text{-}6}$ have calculated VDEs of 0.74 eV, 1.16 eV, 1.45 eV, 1.50 eV, 1.87 eV, and 2.09 eV respectively. Relative energetics suggests that water molecules prefer to interact cohesively instead of binding to the heterocycle at multiple sites.

5.2 Hydrated Pyridazine, Pyrimidine, and Pyrazine Anions

For the hydrated diazine series, the position of the two nitrogen atoms plays an important role in the solvation of the anion with each sequential hydration. Unlike the stable Tz cluster anion, all three of the diazine (Pd, Pm and Pz) monomeric anions are unstable with respect to autodetachment of the excess electron. However, with the addition of a single water molecule, the energy of the hydrated cluster anion becomes lower than that of the corresponding neutral molecular cluster. Only one structure for each of the monohydrated diazines, $A^{-}\cdot(H_2O)$ was found, with computed VDEs of 0.61 eV, 0.59 eV, and 0.69 eV for Pd, Pm and Pz, respectively at the M06-2X/6-31++G(*d*,*p*) level of theory. Stepwise hydration of each negatively charged diazine, $A^{-}\cdot(H_2O)_n$, results in increasing VDEs. Interestingly, the hydrated Pm cluster anions, $Pm^{-}\cdot(H_2O)_n$, have lower computed VDEs than those of the hydrated Pz and Pd cluster anions for the same value of *n*. Structures exhibiting proton transfer have computed VDEs up to 0.7 eV higher in energy than the VDEs of analogous cluster anions of the same size not exhibiting proton transfer. However, structures displaying proton transfer from a hydrogen bonded water molecule to diazine cluster anion are not the lowest energy minima.

5.3 Hydrated Pyridine Anions

Dozens of low-lying minimum energy structures were identified for the negatively charged hydrated pyridine series, and many of them exhibit proton transfer. For *n*=3, even though the lowest energy structure exhibits proton transfer (shown in Figure 4), a structure only 0.08 kcal/mole higher in energy ($Py^-\cdot(H_2O)_3$, shown in Figure 4) does not. For *n*=4-6, the lowest energy structures possess a transferred proton from a water molecule and have VDEs of 1.67 eV, 1.87 eV, and 2.07 eV, respectively. These are shown in Figure 5. The corresponding lowest energy structures with intact water molecules lie at least 1 kcal mol^{-1} higher in energy and have computed VDEs of 1.13 eV, 1.33 eV, and 1.51 eV, respectively. For structures exhibiting proton transfer, only a single deprotonated water molecule interacts directly with the heterocycle. As for the water molecules, a hydrogen-bonded network is formed around the deprotonated water molecule.

6.6Discussion

6.1 Assignment of Experimental PES Features

The combination of negative ion photoelectron spectroscopy with density functional theory provides insight into the important molecular interactions at play in negatively charged cluster anions. In the case of the N-heterocyclic molecular anion clusters studied here, two types of structural motifs are theoretically predicted to result with the attachment of an excess electron. In one case, the excess electron density primarily resides in a * orbital with more than a single water molecules solvating the anion at a single nitrogen atom of the heterocycle: $A\cdot(H_2O)_n + e^- \rightarrow A^-\cdot(H_2O)_n$ results. A secondary phenomenon involves the transfer of a proton from solvent to solute: $A\cdot(H_2O)_n + e^- \rightarrow [AH\cdot OH]^-\cdot(H_2O)_{n-1}$. Table I summarizes the experimental and theoretical results of this study. The quantitative agreement between VDEs computed for the

lowest energy isomers not exhibiting proton transfer, $A^-\cdot(H_2O)_n$, and experiment is better than the proton transfer structures, $[AH\cdot OH]^-\cdot(H_2O)_{n-1}$, for Tz, Pd, Pm, and Pz. This suggests that proton transfer is not occurring in these systems experimentally. In the case of n=3 for Py, however, the same comparison indicates both structural motifs are likely present experimentally. For the Py systems with $n > 3$, VDE data suggests that only structures exhibiting proton transfer, $[PyH\cdot OH]^-\cdot(H_2O)_{n-1}$, are present experimentally.

Table 5.1: Computed VDEs for the lowest energy structural isomers for $A^-\cdot(H_2O)_n$ and $[AH\cdot OH]^-\cdot(H_2O)_{n-1}$ (A = Tz, Pd, Pm, Pz, and Py), the energy difference (in kcal mol^{-1}) between these isomers, and experimental EAs and VDEs.

		Theoretical			Experimental	
	n	$A^-\cdot(H_2O)_n$ VDE	$[AH\cdot OH]^-\cdot(H_2O)_{n-1}$ VDE	E_{rel}	EA	VDE
	1	0.74	---	---	0.38	0.68
	2	1.16	---	---	0.72	1.01
Tz	3	1.45	---	---	1.03	1.41
	4	1.50	2.04	4.20	1.28	1.69
	5	1.87	2.63	1.91	1.43	1.89
	6	2.09	2.84	1.40	1.51	2.09
	1	0.61	---	---	0.40	0.53
	2	1.12	---	---	0.67	0.93
Pd	3	1.46	2.02	6.48	1.09	1.27
	4	1.79	2.37	4.05	1.30	1.53
	5	1.96	2.55	4.14	---	---
	6	1.95	2.79	2.22	---	---

	1	0.59	---	---	0.23	0.42
	2	0.87	---	---	0.62	0.78
Pm	3	1.26	---	---	0.93	1.11
	4	1.36	2.07	3.00	1.16	1.34
	5	1.37	2.34	1.24	1.36	1.58
	6	1.64	2.42	0.00	1.45	1.62
	1	0.69	---	---	0.34	0.66
	2	1.24	---	---	0.73	1.05
Pz	3	1.64	---	---	1.05	1.32
	4	1.67	2.40	2.25	1.31	1.60
	5	1.66	2.55	-3.37	---	---
	6	2.21	2.75	-0.13	---	---
	1	-0.04	---	---	---	---
	2	0.41	---	---	---	---
Py	3	0.84	1.44	-0.02	0.93	0.88, 1.56
	4	1.13	1.70	-1.21	1.23	1.79
	5	1.33	1.87	-4.32	1.48	1.98
	6	1.51	2.07	1.96	1.61	2.18

6.2 Role of Symmetry

S-trazine is the only negatively-charged azabenzene in this study that is stable with respect to autodetachment. The electron affinity was previously reported to be 0.03 eV by Kim and coworkers in 2003.[17] This previous photoelectron spectroscopic study compared the high

symmetry neutral s-triazine (D_{3h}) to the reduced symmetry anion (C_{2v}). A nascent Jahn-Teller distortion has also been recently reported with buckminsterfullerene, C_{60}, with addition of an excess electron perturbing the electronic structure.[54-59] This structural change transforms a number of chemical properties including but not limited to electron affinity, vertical detachment energy, electronic state, charge distribution, and relative energetics between isomers.

The diazines (Pd, Pm, Pz) maintain symmetric geometry of the neutral state upon excess electron attachment. The 1,4 diazine monomer has D_{2h} symmetry in the neutral state where both the 1,3 and 1,2 diazine monomers have C_{2v}. The diazine monomeric symmetry is not altered upon sequential addition of water molecules. Wen et al. suggest that "spherically symmetric" solvents allow for potential energy surfaces to be less affected by solvation, but in our case, water is an asymmetric solvents containing a charge anisotropy giving rise to highly directional noncovalent interactions.[60] It is interesting to point out that pyridazine molecule has neighboring nitrogen atoms in the ring and also theoretically requires only three water molecules to exhibit proton transfer. The quantitative comparison of theory to experiment strongly suggests that proton transfer does not occur in this system. The computed VDEs of the negatively charged clusters that do not exhibit proton transfer agree well with the experiment.

6.3 Extrapolation of the Electron Affinities of the Azabenzenes

Tz is the only azabenzene considered here that exhibits a stable valence bound anion with respect to autodetachment and has a reported EA of 0.03 eV.[17] We recently used the experimental EAs of the negatively charged hydrated Pm series to extrapolate an EA of -0.2 eV for Pm.[15] This value agrees very well with the earlier electron transmission spectroscopy measurement of -0.25 eV. A similar extrapolation for Pd, Pz, and Py using the experimental EAs presented here yields EAs of ~0.0 eV, -0.1 eV, and -0.5 eV respectively. The electron affinity

of the pyridine monomer is in agreement with the previously measured electron transmission spectroscopic (ETS) value of -0.67 eV.[13]

1. Conclusions

Several theoretical studies, including Reimers and Cai, depicted neutral hydrated azabenzene clusters exhibiting proton coupled electron transfer (PCET) in low-lying electronic states for the n, * transition.[61-63] Here, PES elucidates the "linear" hydrogen-bonding motif that is mentioned by Reimers as the dominant monohydrate for all stable azabenzene anions. The PCET monohydrated azines were not present in experimental photoelectron spectra for the corresponding negative ion. Upon sequential hydration, select heterocycles exhibited a shifted higher energy electron binding energy due to PCET. Our technique used in characterizing charge transfer for the hydrated azabenzene anions has been well established and accepted in the field of photoelectron spectroscopy.[51,52,64-72]

The addition of three water molecules is needed to stabilize an excess electron for the pyridine anion due to its more negative electron affinity. Interestingly, the proton transfer species that create a ion complex that maximizes the number of hydrogen bonded water molecules and closely resemble structures previously described by Kim and coworkers.[5] When two nitrogen atoms are present, the stabilization effects of only a single water molecule results in a positive electron affinity.

2. Acknowledgements

This material is partially based (experimental) on work supported by the National Science Foundation under grant nos. _____ and _____ (K.H.B.). This material is partially based (computational) on work supported by the National Science Foundation under

grant no. CHE-1338056 (G.S.T.) and CHE-0955550 (N.I.H). Both G.S.T. and N.I.H. acknowledge EPSCoR support under grant no. EPS-0903787.

(1) Abraham, M. H. *Chem. Soc. Rev.* 1993, *22*, 73.

(2) Desfrançois, C.; Carles, S.; Schermann, J. P. *Chemical Reviews* 2000, *100*, 3943.

(3) Hobza, P.; Šponer, J. *Chemical Reviews* 1999, *99*, 3247.

(4) Kim, K. S.; Tarakeshwar, P.; Lee, J. Y. *Chemical Reviews* 2000, *100*, 4145.

(5) Lee, H. M.; Tarkeshwar, P.; Kim, K. S. *The Journal of Chemical Physics* 2004, *121*, 4657.

(6) Wahl, M. C.; Sundaralingam, M. *Trends in biochemical sciences* 1997, *22*, 97.

(7) Xantheas, S. S. *Chemical Physics* 2000, *258*, 225.

(8) Nakano, S.-i.; Chadalavada, D. M.; Bevilacqua, P. C. *Science* 2000, *287*, 1493.

(9) Petersen, P. B.; Saykally, R. J. *Annu. Rev. Phys. Chem.* 2006, *57*, 333.

(10) Shen, Y. R.; Ostroverkhov, V. *Chemical Reviews* 2006, *106*, 1140.

(11) Eisenberg, D. S.; Kauzmann, W. *The structure and properties of water*; Oxford University Press, 2005.

(12) Scheiner, S. *Hydrogen bonding. A theoretical perspective*, 1997.

(13) Nenner, I.; Schulz, G. *The Journal of Chemical Physics* 1975, *62*, 1747.

(14) Periquet, V.; Moreau, A.; Carles, S.; Schermann, J.; Desfrancois, C. *Journal of Electron Spectroscopy and Related Phenomena* 2000, *106*, 141.

(15) Kelly, J. T.; Xu, S.; Graham, J.; Nilles, J. M.; Radisic, D.; Buonaugurio, A. M.; Bowen Jr, K. H.; Hammer, N. I.; Tschumper, G. S. *The Journal of Physical Chemistry A* 2014.

(16) Han, S. Y.; Chu, I.; Kim, J. H.; Song, J. K.; Kim, S. K. *The Journal of Chemical Physics* 2000, *113*, 596.

(17) Kim, J. H.; Song, J. K.; Park, H.; Lee, S. H.; Han, S. Y.; Kim, S. K. *The Journal of chemical physics* 2003, *119*, 4320.

(18) Song, J. K.; Lee, N. K.; Kim, S. K. *The Journal of chemical physics* 2002, *117*, 1589.

(19) Kamrath, M. Z.; Relph, R. A.; Johnson, M. A. *Journal of the American Chemical Society* 2010, *132*, 15508.

(20) Lee, S. H.; Kim, N.; Ha, D. G.; Kim, S. K. *Journal of the American Chemical Society* 2008, *130*, 16241.

(21) Coe, J.; Snodgrass, J.; Freidhoff, C.; McHugh, K.; Bowen, K. *The Journal of chemical physics* 1986, *84*, 618.

(22) Neumark, D.; Lykke, K.; Andersen, T.; Lineberger, W. *Physical Review A* 1985, *32*, 1890.

(23) Siegel, M.; Celotta, R.; Hall, J.; Levine, J.; Bennett, R. *Physical Review A* 1972, *6*, 607.

(24) Travers, M. J.; Cowles, D. C.; Ellison, G. B. *Chemical physics letters* 1989, *164*, 449.

(25) Frisch, M. J.; Trucks, G. W.; Schlegel, H. B.; Scuseria, G. E.; Robb, M. A.; Cheeseman, J. R.; Scalmani, G.; Barone, V.; Mennucci, B.; Petersson, G. A.; Nakatsuji, H.; Caricato, M.; Li, X.; Hratchian, H. P.; Izmaylov, A. F.; Bloino, J.; Zheng, G.; Sonnenberg, J. L.; Hada, M.; Ehara, M.; Toyota, K.; Fukuda, R.; Hasegawa, J.; Ishida, M.; Nakajima, T.; Honda, Y.; Kitao, O.; Nakai, H.; Vreven, T.; Montgomery Jr., J. A.; Peralta, J. E.; Ogliaro, F.; Bearpark, M. J.; Heyd, J.; Brothers, E. N.; Kudin, K. N.; Staroverov, V. N.; Kobayashi, R.; Normand, J.; Raghavachari, K.; Rendell, A. P.; Burant, J. C.; Iyengar, S. S.; Tomasi, J.; Cossi, M.; Rega, N.; Millam, N. J.; Klene, M.; Knox, J. E.; Cross, J. B.; Bakken, V.; Adamo, C.; Jaramillo, J.; Gomperts, R.; Stratmann, R. E.; Yazyev, O.; Austin, A. J.; Cammi, R.; Pomelli, C.; Ochterski, J.

W.; Martin, R. L.; Morokuma, K.; Zakrzewski, V. G.; Voth, G. A.; Salvador, P.; Dannenberg, J. J.; Dapprich, S.; Daniels, A. D.; Farkas, Ö.; Foresman, J. B.; Ortiz, J. V.; Cioslowski, J.; Fox, D. J.; Gaussian, Inc.: Wallingford, CT, USA, 2009.

(26) Zhao, Y.; Truhlar, D. G. *Theoretical Chemistry Accounts* 2008, *120*, 215.

(27) Zhao, Y.; Truhlar, D. G. *Accounts of Chemical Research* 2008, *41*, 157.

(28) Zhao, Y.; Truhlar, D. G. *The Journal of Physical Chemistry A* 2008, *112*, 1095.

(29) Howard, J. C.; Hammer, N. I.; Tschumper, G. S. *ChemPhysChem* 2011, *12*, 3262.

(30) Allodi, M. A.; Dunn, M. E.; Livada, J.; Kirschner, K. N.; Shields, G. C. *The Journal of Physical Chemistry A* 2006, *110*, 13283.

(31) Anderson, J. A.; Tschumper, G. S. *The Journal of Physical Chemistry A* 2006, *110*, 7268.

(32) Bates, D. M.; Smith, J. R.; Janowski, T.; Tschumper, G. S. *The Journal of Chemical Physics* 2011, *135*.

(33) Bates, D. M.; Smith, J. R.; Tschumper, G. S. *Journal of Chemical Theory and Computation* 2011, *7*, 2753.

(34) Bates, D. M.; Tschumper, G. S. *The Journal of Physical Chemistry A* 2009, *113*, 3555.

(35) Dahlke, E. E.; Olson, R. M.; Leverentz, H. R.; Truhlar, D. G. *The Journal of Physical Chemistry A* 2008, *112*, 3976.

(36) Shields, R. M.; Temelso, B.; Archer, K. A.; Morrell, T. E.; Shields, G. C. *The Journal of Physical Chemistry A* 2010, *114*, 11725.

(37) Hammer, N. I.; Roscioli, J. R.; Bopp, J. C.; Headrick, J. M.; Johnson, M. A. *The Journal of chemical physics* 2005, *123*, 244311.

(38) Asmis, K. R.; Santambrogio, G.; Zhou, J.; Garand, E.; Headrick, J.; Goebbert, D.; Johnson, M. A.; Neumark, D. M. *The Journal of chemical physics* 2007, *126*, 191105.

(39) Ayotte, P.; Bailey, C. G.; Kim, J.; Johnson, M. A. *Journal of Chemical Physics* 1998, *108*, 444.

(40) Ayotte, P.; Johnson, M. A. *The Journal of chemical physics* 1997, *106*, 811.

(41) Bailey, C. G.; Kim, J.; Johnson, M. A. *The Journal of Physical Chemistry* 1996, *100*, 16782.

(42) Kim, J.; Becker, I.; Cheshnovsky, O.; Johnson, M. A. *Chemical physics letters* 1998, *297*, 90.

(43) Kim, J.; Park, J. M.; Oh, K. S.; Lee, J. Y.; Lee, S.; Kim, K. S. *The Journal of chemical physics* 1997, *106*, 10207.

(44) Kim, K. S.; Park, I.; Lee, S.; Cho, K.; Lee, J. Y.; Kim, J.; Joannopoulos, J. *Physical review letters* 1996, *76*, 956.

(45) Lee, H. M.; Lee, S.; Kim, K. S. *The Journal of chemical physics* 2003, *119*, 187.

(46) Posey, L. A.; Johnson, M. A. *The Journal of chemical physics* 1988, *89*, 4807.

(47) Robertson, W. H.; Diken, E. G.; Price, E. A.; Shin, J.-W.; Johnson, M. A. *Science* 2003, *299*, 1367.

(48) Roscioli, J.; Johnson, M. *The Journal of chemical physics* 2007, *126*, 024307.

(49) Roscioli, J. R.; Hammer, N. I.; Johnson, M. *The Journal of Physical Chemistry A* 2006, *110*, 7517.

(50) Puiatti, M.; Vera, D. M. A.; Pierini, A. B. *Physical Chemistry Chemical Physics* 2008, *10*, 1394.

(51) Desfrancois, C.; Baillon, B.; Schermann, J.; Arnold, S.; Hendricks, J.; Bowen, K. *Physical review letters* 1994, *72*, 48.

(52) Haranczyk, M.; Bachorz, R.; Rak, J.; Gutowski, M.; Radisic, D.; Stokes, S. T.; Nilles, J. M.; Bowen, K. H. *The Journal of Physical Chemistry B* 2003, *107*, 7889.

(53) Wang, X.-B.; Kass, S. R. *Journal of the American Chemical Society* 2014, *136*, 17332.

(54) Green, W. H.; Gorun, S. M.; Fitzgerald, G.; Fowler, P. W.; Ceulemans, A.; Titeca, B. C. *The Journal of Physical Chemistry* 1996, *100*, 14892.

(55) Kato, T.; Kodama, T.; Shida, T. *Chemical physics letters* 1993, *205*, 405.

(56) Koga, N.; Morokuma, K. *Chemical physics letters* 1992, *196*, 191.

(57) Voora, V. K.; Cederbaum, L. S.; Jordan, K. D. *The Journal of Physical Chemistry Letters* 2013, *4*, 849.

(58) Wang, X.-B.; Woo, H.-K.; Wang, L.-S. *The Journal of chemical physics* 2005, *123*, 051106.

(59) Zakrzewski, V. G.; Dolgounitcheva, O.; Ortiz, J. V. *The Journal of Physical Chemistry A* 2014.

(60) Wen, H.; Hou, G.-L.; Kathmann, S. M.; Valiev, M.; Wang, X.-B. *The Journal of Chemical Physics* 2013, *138*.

(61) Liu, X.; Sobolewski, A. L.; Borrelli, R.; Domcke, W. *Physical Chemistry Chemical Physics* 2013, *15*, 5957.

(62) Liu, X.; Sobolewski, A. L.; Domcke, W. *The Journal of Physical Chemistry A* 2014, *118*, 7788.

(63) Reimers, J. R.; Cai, Z.-L. *Physical Chemistry Chemical Physics* 2012, *14*, 8791.

(64) Dąbkowska, I.; Rak, J.; Gutowski, M.; Nilles, J. M.; Stokes, S. T.; Bowen Jr, K. H. *The Journal of chemical physics* 2004, *120*, 6064.

(65) Dąbkowska, I.; Rak, J.; Gutowski, M.; Nilles, J. M.; Stokes, S. T.; Radisic, D.; Bowen Jr, K. H. *Physical Chemistry Chemical Physics* 2004, *6*, 4351.

(66) Eustis, S. N.; Radisic, D.; Bowen, K. H.; Bachorz, R. A.; Haranczyk, M.; Schenter, G. K.; Gutowski, M. *Science* 2008, *319*, 936.

(67) Gutowski, M.; Dabkowska, I.; Rak, J.; Xu, S.; Nilles, J.; Radisic, D.; Bowen Jr, K. *The European Physical Journal D-Atomic, Molecular, Optical and Plasma Physics* 2002, *20*, 431.

(68) Haranczyk, M.; Dąbkowska, I.; Rak, J.; Gutowski, M.; Nilles, J. M.; Stokes, S.; Radisic, D.; Bowen, K. H. *The Journal of Physical Chemistry B* 2004, *108*, 6919.

(69) Harańczyk, M.; Gutowski, M.; Li, X.; Bowen, K. H. *Proceedings of the National Academy of Sciences* 2007, *104*, 4804.

(70) Haranczyk, M.; Rak, J.; Gutowski, M.; Radisic, D.; Stokes, S. T.; Bowen, K. H. *The Journal of Physical Chemistry B* 2005, *109*, 13383.

(71) Harańczyk, M.; Rak, J.; Gutowski, M.; Radisic, D.; Stokes, S. T.; Bowen, K. H. *Israel journal of chemistry* 2004, *44*, 157.

(72) Mazurkiewicz, K.; Haranczyk, M.; Gutowski, M.; Rak, J.; Radisic, D.; Eustis, S. N.; Wang, D.; Bowen, K. H. *Journal of the American Chemical Society* 2007, *129*, 1216.

Appendix I Updated Bleeding Procedure of Ultra-High Vacuum Chambers

Mechanical Pump and Sorption Pump Preparation

An additional mechanical pump is needed to pump on the sorption pumps and to rough out Chambers 3, 4, and 5 during the pump down. It can be completed one day prior to the bleeding process. A variacs, thermometer, heating cuff, and liquid nitrogen container for each sorption pump is needed. Sorption pump baking can be completed one day prior to the operation or during the bleed.

1. *Turn on the third mechanical pump.* Connect the third mechanical pump to a valve leading to the sorption pumps and to a valve leading to the Chambers 3, 4, and 5 roughing bus. Refer to the sketch. Turn on the third mechanical pump. Fill the small liquid nitrogen (LN_2) trap and pump out the line to the sorption pumps. Pump out the sorption pumps one at a time to 100 – 200 mtorr, then pump all three to 20 mtorr.

2. *Bake the sorption pumps.* Start warming up the sorption pumps using the heating cuffs each attached to a variac. Slowly warm up the heating cuffs. To bake the sorption pumps faster, start at 100 V on the variacs. Monitor the temperature of the cuffs using a thermometer. Building Scientific Apparatus instructs to bake the sorption pumps to 250 °C. The sorption pumps should be heated for at least five hours. The mechanical pump may reach 1000 mtorr. Eventually the pressure should then decline to about 20 mtorr.

3. *Cool sorption pumps to room temperature.* The sorption pumps need to cool overnight for about 24 hours.to room temperature before they can be cooled with liquid nitrogen.

4. *Cool sorption pumps with liquid nitrogen.* Make sure the pressure on the sorption pumps is low (~20 mtorr), otherwise the mechanical pump oil might be absorbed by sorption pumps. During the pump down, open the third mechanical pump to the sorption pumps and start cooling them with liquid nitrogen. Hook the insulating liquid nitrogen containers to the sorption pumps and fill them with liquid nitrogen. This devise acts like a buffer in case the mechanical pump oil backstream into the sorption pump.

5. *Open sorption pumps to the machine.* Top off the liquid nitrogen levels. Close the sorption pump valve to the mechanical pump and open the sorption pump valve to the Chambers 3, 4, and 5 roughing bus.

6. *Top off the liquid nitrogen levels.* About every hour, refill the liquid nitrogen containers that cool the sorption pumps. Keep track of how many times the 1 L dewar is refilled.

7. *Close off the sorption pumps to the chambers.* Once the pressure in the chambers on the high vacuum side of the machine are in the 10^{-7} torr range, close off the sorption pumps to the chambers.

8. *Warm the sorption pumps to room temperature.* Remove the liquid nitrogen containers from the sorption pumps and check that the sorption pumps are warming up.

9. *Open sorption pumps to the mechanical pump.* After about an hour, open the sorption pumps to the mechanical pump to get rid of some of the adsorbed gas.

10. *Turn off the mechanical pump.* Once the sorption pumps have warmed to room temperature (at least 0 °C where the ice starts to melt), turn off the mechanical pump to the sorption pumps.

Bleed

1. *Set the N_2 regulator pressure.* Prior to starting the bleed, be sure the N_2 tank with the regulator is in position and has been tested for leaks using the Snoop leak detector. For a quicker bleed, set the regulator for about 20 – 30 psi. A leak valve may be used.

2. *Install needle gauge on Chamber 0.* Normal bleed of the top of Chambers 0, 1, and 2 to install the gauge and stopper piece using the ultra torr port where the filament controls are usually located.

3. *Normal SNIPES pump down.* Use the mechanical pumps to rough out the top of Chambers 0, 1, and 2 like the normal SNIPES pump down as if running. Once the diffusion pumps have warmed up, use the diffusion pumps to pump on Chambers 0, 1, and 2.

4. *Open the in-line gate valve.* Once the pressure is low enough (Chamber 0: ~5 x 10^{-6} torr; Chambers 1 and 2: ~2 x 10^{-6} torr), open the in-line gate valve. Turn ionization gauges and

ion pumps off. Close the diffusion pumps to the chambers. This practice is aimed to have the mid vacuum (Ch0,1, and 2) and high vacuum (Ch3, 4, and 5) in the relatively same vacuum level. Otherwise atmosphere gas molecules especially water will get into the high vacuum chambers and it is ruining the purpose of N2 bleeding.

5. *Start the N_2 bleed.* Attach the N_2 gas line to Chamber 0 through the bleed valve. The vacuum was used to hold a stopper that fits just inside the bleed valve. Wait for the pressure to rise to atmosphere by monitoring the N_2 regulator and the newly installed needle gauge. One should be very patient during this process. If the N2 bleeding going too fast it might end up having the pressure inside the chamber higher than the atmosphere and thus ruins the gold seal in chamber 5. The bleed should take at least two hours and may take longer.

6. *Finish the bleed.* Once the machine has been bled and the pressure gauge reads 0 inHg, check to see if the stopper device that was installed on Chamber 0 is able to be easily lifted off the cylindrical base. If so, the machine pressure is up to atmospheric pressure and now the repair can start. If the stopper is not able to be lifted, wait a little longer and check again. The stopper will easily come off once there is no longer vacuum pressure holding it in place, or when the pressure inside equals the pressure outside the instrument.
7. *Close the N_2 bleed valve and N_2 tank*. Start the repair or improvement work on the high vacuum side. Once the ultrahigh vacuum is open, N_2 should be continuously flowed through the machine if desired.

8. *Cool sorption pumps with liquid nitrogen.* Make sure the pressure on the sorption pumps is low (~20 mtorr). Open the mechanical pump to the sorption pumps and start cooling them with liquid nitrogen. Hook the insulating liquid nitrogen containers to the sorption pumps and fill them with liquid nitrogen.

9. *Open the mechanical pumps to the chambers.* Check to make sure the N_2 tank is closed to the machine. Wait for the pressures to equilibrate and then slowly open the Chamber 0 mechanical pump to the chambers. Monitor the pressure using the needle gauge on Chamber 0 until the pressure is low enough to use the thermocouple gauge. From atmospheric pressure to 1000 mtorr is the critical pressure range. It may take about an hour with only the Chamber 0 mechanical pump. Then, open the Chamber 1 and 2 mechanical pump. The in-line gate valve should still be open.

   Note: After the machine is roughed out, the rest of the pump down procedures can wait until the next day. Then the next day rough out the chambers and the diffusion pumps.

   Note: If pumping down in the same day, close the forelines to the diffusion pumps and pump on the entire machine. This will take a lot of cycling between diffusion pump forelines and the top of the chamber. If pumping down in the same day, it is suggested to wait to turn on the diffusion pumps until after the machine has been roughed out to avoid repetitive cycling.

10. *Double pump.* Turn on the diffusion pumps and wait for them to warm up. Rough out the diffusion pumps and the top of the chamber using the mechanical pumps as usual (once the pressure reaches ~200 mtorr). This is the usual SNIPES pump down but the in-line gate valve should be open.

11. *Open diffusion pumps, turn on ion gauges, cool sorption pumps.* Open the diffusion pumps to Chambers 0, 1, and 2. Turn on, then off, then on the Chambers 0, 1, and 2 ion gauges. Start cooling the sorption pumps with liquid nitrogen.

12. *Open sorption pumps to chambers.* After about an hour, close the sorption pump valve to the third mechanical pump. Open the sorption pumps to the Chambers 3, 4, and 5 roughing bus.
13. *Open the gold seals.* Open the Chambers 3 and 4 gold seal (refer to the sketch) and make sure the pressures are alright. Then open the Chamber 5 gold seal. The sorption pumps are now pumping on Chambers 3, 4, and 5. Twenty-nine full turns of the gold seal mean that it is fully open. The gold seals have a built in stop to prevent them from opening too far.

14. *Turn on high vacuum ion gauges.* Turn on the Chambers 3, 4, and 5 ion gauges and monitor the pressures.

15. *Refill liquid nitrogen levels.* Top up the sorption pump liquid nitrogen about every hour. Also check the liquid nitrogen trap level.

16. *Leak check where the machine was repaired.* Acetone leak check the bolts that were re-tightened after entering the machine. Spray acetone on the flange and if the pressure in the chamber rises, there is a leak and the bolts need to be tightened. After tightening the bolts, the pressure then should drop.

17. *Cycle the Chamber 3 and 4 ion pumps, then turn them on.* Once the pressure in Chamber 3 reaches the mid 10^{-6} torr range, cycle the Chambers 3 and 4 ion pumps on and off repeatedly until the current comes down and stays on the scale. Check the temperature of the ion pumps to make sure they are not too warm. The pressure in Chambers 3, 4, and 5 may rise to ~10^{-4} torr. Wait for the pressure to come back down to where it was before cycling the ion pumps. Then try cycling the ion pumps again.

    Note: The Chamber 3 ion pump stayed on when the pressure was 1.5 x 10^{-6} torr and the Chamber 4 ion pump stayed on when the pressure was 3.0 x 10^{-6} torr.

18. *Cycle the Chamber 5 ion pumps, then turn them on* When the Chamber 5 pressure reaches the low 10^{-5} torr range, turn on the Chamber 5 ion pump. If the pressure rises to ~10^{-4} torr, turn off the ion pump manually. Turn on and off the Chamber 5 ion pump until the current stays down and the pressure stays down. Monitor the temperature of the bays on the pump and if they get too warm, turn off the ion pump to let them cool. Cycle the ion pump.

19. *Close the in-line gate valve.* Once the Chamber 5 ion pump is able to stay on, make sure the pressure continues to decrease. Close the in-line gate valve and check the pressures again. Re-open the in-line gate valve and be sure that the pressure in Chamber 3 begins to rise. Close the in-line gate valve and make sure the pressure in Chamber 3 drops again.

20. *Turn off sorption pumps and diffusion pumps, check the ion pumps.* Turn off the sorption pumps to the machine and drop the liquid nitrogen containers from the sorption pumps. Make sure the in-line gate valve is closed and turn the diffusion pumps off. Check that the sorption pumps are warming back up to room temperature. All the ion pumps should be in protection mode at this point.

21. *Close the gold seals.* Once the ion pumps are alright, close the gold seals with 6 foot-pounds of torque.

22. *Open the third mechanical pump to the sorption pumps.* Open the sorption pumps to the mechanical pump to get rid of the gas as they begin to warm up. About an hour after the diffusion pumps were turned off, turn off the mechanical pumps to Chambers 0, 1, and 2. When the ice on the sorption pumps begins to melt, they are at 0 °C. Leave the mechanical pump on for about another hour and then turn off the mechanical pump for the sorption pumps.

23. *Check pressure gauges and pumps.* Make sure the pressures in Chambers 3, 4, and 5 are headed in the right direction and proceed with normal shut down procedures. Double

check that all the mechanical, diffusion, and sorption pumps are turned off. Make sure the diffusion pump water is turned off (an hour after the diffusion pumps are turned off). Continue to monitor the pressures, especially in Chamber 5. Triple check all the gauges as usual. If the Chamber 5 pressure does not reach ~2 x 10^{-9} torr within the next few weeks, the chamber may have to bake to get rid of any gas physisorbed to the surfaces. Baking the chamber should eventually allow it to reach the desired pressure.

Appendix II Fix of loosen Faraday cup and Modifiation.

After the machine was bled with N_2 (which took four hours), the blank-off Conflat flange below the Faraday cup, two side feed-through flanges, and the flange with the bellows actuator were removed. The side feed-through flange with the electrical connection had to be removed careful to not disrupt the connections. Three screws came out. The initial problem was therefore that the screws had loosened over time which eventually caused them to fall out and disconnect the Faraday cup from the bellows actuator. The bellows manipulator allows the Faraday cup to be moved up and down on a daily basis. It was difficult to maneuver the Faraday cup arm because it was stuck on the ledge inside Chamber 3. The Faraday cup assembly did not fit through the chamber tube so the Faraday cup was detached from the arm. The electrical connections including the nuts from the threaded rod were also disconnected. Two screws were removed.

Once all of the Faraday cup parts were removed from the chamber, some machining modifications were necessary in order to get the Faraday cup assembly to fit back into the chamber without disconnecting the chamber from the machine (which would require extremely careful aligning and thus was to be avoided). The Faraday cup housing and other pieces were modified in order to get the assembly to fit through the tube. The overall reduction in the housing to shield horizontal direction was 0.250 inches. Once all the modifications were made and the screws were tightened, the assembly was put back into Chamber 3. The Faraday cup assembly was reattached to the top conflate flange and the electrical connection was made to the feed-through flange. The electrical connectivity was verified by checking the resistance using the ohmmeter setting of a multimeter. In the ‘down’ position, the Faraday cup connectivity gave a reading because the Faraday cup is isolated. In the ‘up’ position, the Faraday cup was grounded as was expected and correct. The connections were secure and stable after a few up and down

movements. The ports were closed by tightening the bolts in a star pattern. This ensured that the knife edges would slowly and evenly bite into the OFC (oxygen free copper) gasket. The ports were closed and then the pump down process began.

The stainless steel Faraday cup housing was 1 inch long but 0.120 inches were removed leaving it 0.880 inches long. The space between the top of the Faraday cup and the housing was 0.209 inches before the 0.120 inches were removed from the housing. The vespel insulator just behind the Faraday cup is 0.070 inches thick. The vespel insulator on the other side of the arm was 0.192 inches thick and then at least 0.120 inches were removed leaving it between 0.050 and 0.070 inches thick. The all thread was shortened by 0.16 inches. The overall reduction was 0.240 inches from the vespel insulator and the stainless steel housing. Once these modifications were made, the nut on the all thread and the two screws holding the housing touched. Therefore, the screw heads were countersunk into the arm resulting in no contact. The Faraday cup got stuck when it was put down the tube so another 10 microns (0.010 inches) from the housing had to be removed. Once this was removed, the Faraday cup apparatus was able to make it past the weld seam inside the machine. Please see the blueprints for the current measurements.

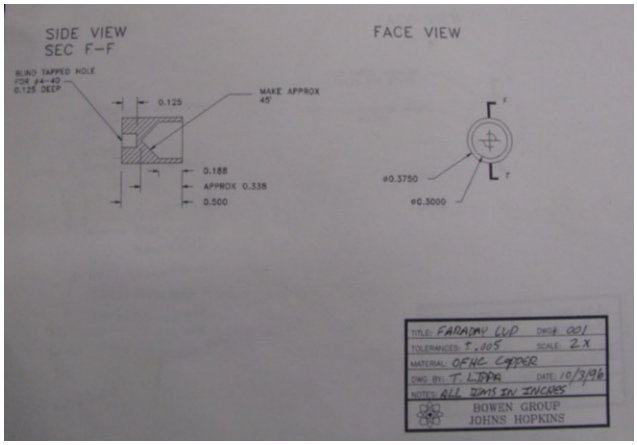

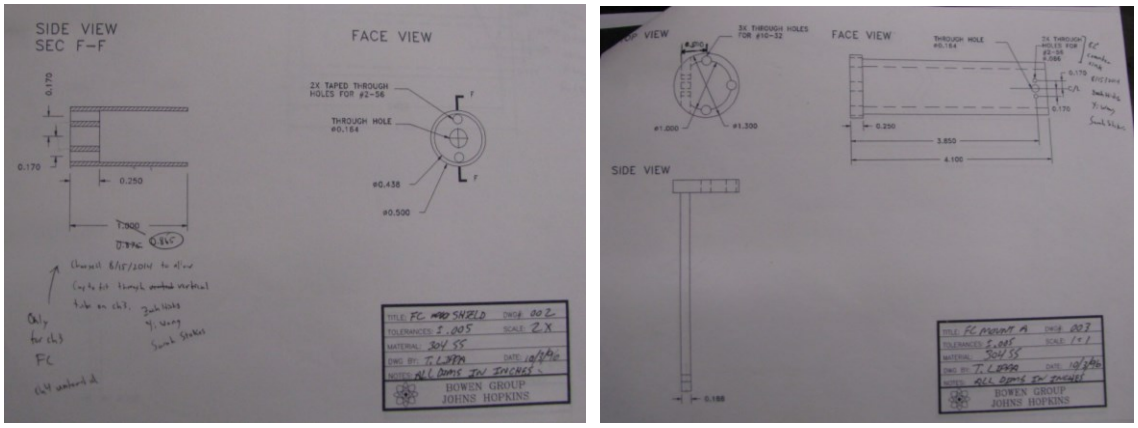

Figure A1Redesign of the Faraday Cup

Appendix III Coupling Mass Spectrometry with Computer

Background

In order to collect a photoelectron spectrum accurately, precisely mass-selecting the cluster anion is one of the important step. Mass spectrum alone can provide critical information of the molecule/cluster ions to be analyzed. For instance, the intensity of the peaks can tell us the information about the stability of certain species, and sometimes, given the isotope pattern, the composition of the molecule/cluster ions can be determined. In publications, a clean and well calibrated mass spectrum is desirable. Since the magnetic sector mass spectrometer equipped on SNIPES is a home-made apparatus, it provides the opportunity that one can have much more freedom than the commercial ones to optimize its performance, including sensitivity, resolution, and noise-to-signal ratio. However, it is also challenging at the same time.

System Overview

The mass spectrometer equipped on SNIPES consist of Nuclide Magnet Regulator, Keithley 2000 Digital Multimeter, and the Krithley 6514 Digital Electrometer. The data acquisition program is Labview Signal Express, download available at National Instrument website. Nuclide Magnet Regulator controls the current going through the copper coils in the magnet, thus the magnitude of magnetic field. The Nuclide Magent Regulator has two modes, manual and scan mode. Setting at manual mode, one can scan the mass spectrometer to search for mass signal. By setting at scan mode, one can scan the whole mass spectrum with a constant rate of increasing magnetic field. Keithley 2000 Digital Multimeter is used to read the voltage on the Hall probe, installed on the magnetic sector. The working principle of Hall probe is when electric current is passing through a conductor placed in a magnetic field, due to the Hall effect, the charge on the conductor will be separated along the perpendicular direction to the current. Therefore, measuring the voltage difference can thus give the magnitude of the magnetic field.

Using the Keithley 2000 Digital Multimeter, a roughly 400 pA noise level incurs. However, acquiring data by the chart recorder, the noise is filtered out due to the slow response of the chart recorder. In order to acquire data by Labview program, a signal amplifier was used so that the signal to noise level can be optimized.

System Operation

Using Chart Recorder

In this section, the procedure of collecting mass spectrum using chart recorder is described. This is only for the circumstances that the computerized mass spectrometer is not working. Using the chart recorder can be a good method in the trouble-shooting stage. The chart recorder simply records the signal collected through the picoameter versus the time. When collecting the mass spectrum, switch the operation mode on the Nuclide Magnet Regulator to "scan mode," the magnetic field will be increasing as the function of current. Along the mass scanning phase, one should watch the chart recorder and the hall probe electrometer very closely. When there is a peak shows up on the chart recorder, one should record the voltage on the hall probe immediately, for the future mass identification and calibration. For a better mass calibration, one should go back to the manual mode and search for the peaks on the mass spectrum, to record the more precise peak position. This is a disadvantage of the chart recorder - it requires one person to watch the chart recorder through the collection. Also due to the imperfect time coordination of human beings, recording the peak position precisely is nearly impossible. There are some variation can be made on the chart recorder. Rolling rate can be adjusted so that one can observe a more detailed or more general looking mass spectrum. Intensity can be adjusted so that the peak can be enlarged or shorten.

Using the Computerized Mass Spectrometer.

When the system is in operation, typically three sets of data are acquired simultaneously, the Hall probe voltage, ion current, and time. The data sets given by the Labview program are Hall probe voltage vs. Time and ion current vs. Time. Back in the old days, we calibrate the mass by comparing the hall probe voltage and ion current. The first step is making the hall probe voltage vs. ion current graph. However, due to the fluctuation of the hall probe voltage reading, the graphs do not look ideal. We smooth the Hall probe reading by fitting Hall probe voltage and the time. Then we use the smoothened hall probe voltage to fit with the ion current, linked by the time. The mass calibration can be done by carefully chose the four peaks with the known mass and make a plot, then do a second order polynomial fit to make the calibration curve.

Future Improvement

Much of the noise and fluctuation on the mass spectra come from the electronic interference inside the chamber 5. Also, we found that the quality and length of the BNC cable connecting the electrometer and the bus card have an impact on the noise level. In order to reduce the noise to signal ratio, a BNC cable of higher quality and of shorter length can be used. Another way to reduce the noise level is acquire a better signal amplifier. As mentioned before, the amplifier can filter the noise. The signal amplifier in use can only amplify the signal 10 folds. The newer model is recommended, which can amplify the signal by 1000 folds.

Another improvement involves more mathematics and Labview programing skills. Presently, the mass calibration is done manually. One has to calibrate the mass spectrum by the known mass peak against the hall probe and/or the time. If the relation between the signal current and hall probe voltage/time is liner, an universal equation can be utilized so that for every mass spectrum collected, one equation can be used to convert the hall probe voltage to the mass.

However, as mentioned in the chapter 1, the relation is 2nd order. Therefore with different scan starting point, the 2nd order equation is different. For future improvement, one can develop an equation that can relate the mass-to-time equation with the scan starting point. Furthermore, this can be implemented into the labview program, so that manually mass calibration can be replaced by the computerized automated mass calibration.

Cumulative Vitae

Yi Wang

| ywang136@jhu.edu | 740-629-3437

EDUCATION

Ph.D. in Chemistry, ***Johns Hopkins University, Baltimore, MD*** ***October, 2015***

Thesis Title: Photoelectron Spectroscopic Study of Cluster Anions
Adviser: Dr. Kit H. Bowen

Bachelor of Science, **Chemistry and Physics,** ***Marietta College, Marietta, OH*** ***May, 2010***

Senior Research Project: Study of Electron-Transfer Quenching Mechanism of a Fluorescence Process
Adviser: Dr. Debra Egolf

RESEAERCH EXPERIENCE

Research Assistant, Dr. Kit Bowen Group

Johns Hopkins University, Chemistry Department, Baltimore MD ***2010-2015***

- Utilize photoelectron spectroscopy technique to investigate the unique stepwise salvation properties of biological molecule clusters anions in gas-phase.
- Investigate the electron induced proton transfer process in DNA-like molecules and performed theoretical calculations independently.
- Used arc pulsed ion source to discover new designer magnetic superatoms.
- Develop and improved several ion sources using techniques including supersonic expansion, laser vaporization, magnetron, and pulsed arc ion sources.
- Redesigned and improved the negative ion detector. Coupled magnetic sector mass spectrometer with computer, largely improved the resolution and signal intesity.
- Maintained and improved the ultra-high vacuum systems.
- Trained the new graduate students and undergraduate researchers.

Undergrad Research Assistant

Marietta College, Marietta, OH ***2009-2010***

- Designed and developed new techniques and method to study of electron-transfer quenching mechanism of a fluorescence process.
- Trained other undergrad students to use varies scientific instruments.

TEACHING EXPERIENCE

Teaching Assistant

Johns Hopkins University, Chemistry Department, Baltimore, MD 2010-2015

- Physical Chemistry Lecture and Laboratory
  Create supplemental course materials discussing current science events and articles.
  Fixed and improved physical chemistry lab equipment.
- General Chemistry Lecture and Laboratory
  Held office hours and help session, supervised lab safety.

PROFESSIONAL AFFILIATIONS

- American Chemical Society
- American Physical Society

PUBLICATIONS

1. **Y. Wang**, X. Zhang, S. Lyapustina, M. Nilles, S. Xu, J. Graham, K. Bowen, J. Kelly, G. Tschumper, and N. Hammer. "The Onset of Electron-Induced Proton-Transfer in Hydrated Azabenzene Cluster Anions" (Submitted)

2. **Y. Wang**, X. Zhang, Z. Hicks, and K. Bowen, "Photoelectron Spectroscopic Study of Caffeine Cluster Anions" (manuscript under development)

3. **Y. Wang**, S. Stokes, X. Zhang, A. Vlk, and K. Bowen, "Electron-Induced Proton Transfer in 2-hydroxypyridine: A Photoelectron Spectroscopic and Density Functional Theory Study" (manuscript under development)

4. X. Zhang, **Y. Wang**, H. Wang, A. Lim, G. Gantefoer, K. H. Bowen, J. U. Reveles, and S. N. Khanna, "On the Existence of Designer Magnetic Superatoms", *J. Am. Chem. Soc.*, 135, 4856 −4861 (2013)

5. A. M. Buytendyk, **Y. Wang**, J. D. Graham, A. K. Kandalam, B. Kiran and K. H. Bowen, "Photoelectron spectrum of a polycyclic aromatic nitrogen heterocyclic anion: quinolone$^-$", *Molecular Physics*. 1-4 (2015)

6. J. Graham, A. Buytendyk, **Y. Wang**, S. K. Kim, and K. H. Bowen "CO2 Binding in the (Quinoline-CO2)- Anionic Complex" *Journal of Chemical Physics* **142**, 234307 (2015).

7. A. Buonaugurio, X. Zhang, S. T. Stokes, **Y. Wang**, G. B. Ellison, K. H. Bowen, "The photoelectron spectrum of the benzaldehyde anion",*Int. J. of Mass Spectrom*., 278–280(2014)

8. J. Lambert, J. Chen, A. Buonaugurio, K. H. Bowen, C. L. Do-Thanh, **Y. Wang**, M. D. Best,

R. N. Compton, and T. Sommerfeld, "Combined photoelectron, collision-induced dissociation, and computational studies of parent and fragment anions of N-paranitrophenyl-sulfonylalanine and N-paranitrophenylalanine",*J. Chem. Phys.* 139, 224308 (2013)

9. L. Chomicz, M. Zdrowowicz, F. Kasprzykowski, J. Rak, A. Buonaugurio, **Y. Wang**, and K. H. Bowen , "How to Find Out Whether a 5-Substituted Uracil Could Be a Potential DNA Radiosensitizer", *J. Phys. Chem. Lett.,* 4 , 2853(2013)

10. X. Zhang, B. Visser, M. Tschurl, E. Collins, **Y. Wang**, Q. Wang, Y. Li, Q. Sun, P. Jena, G. Gantefoer, U. Boesl, U. Heiz, and K. H. Bowen, "In Search of Four-Atom Chiral Metal Clusters", *J. Chem. Phys.* 139, 111101 (2013)

11. X. Tang, X. Li, **Y. Wang**, K. Wepasnick, A. Lim, D. H. Fairbrother, K. H. Bowen, T. Mangler, S. Noessner, C. Wolke, M. Grossmann, A. Koop, G. Gantefoer, B. Kiran and A. K. Kandalam , "Size Selected Clusters on Surfaces", *J. Phys.: Conf. Ser.* 438 0120 (2013)

12. X. Li, K. A. Wepasnick, X. Tang, **Y. Wang**, K. H. Bowen, D. H. Fairbrother,and, G. Gantefoer, "Ion induced modification of size-selected MoO3 and WO3 clusters deposited on HOPG",*J. Vac. Sci. Technol. B* 30, 031806 (2012)

13. B. Kiran, A. K. Kandalam, R. Rallabandi, P. Koirala, X. Li, X. Tang, **Y. Wang**, H. Fairbrother, G. Gantefoer, and K. H. Bowen, "(PbS)32: A baby crystal", *J. Chem. Phys.,* 136, 024317 (2012)